การตรวจสอบความคลาดเคลื่อนในการซ้อนทับภาพของเครื่องวางแผนการรักษา

นางสาวสุมนา สมบูรณ์

วิทยานิพนธ์นี้เป็นส่วนหนึ่งของการศึกษาตามหลักสูตรปริญญาวิทยาศาสตรมหาบัณฑิต
สาขาวิชาฉายาเวชศาสตร์ ภาควิชารังสีวิทยา
คณะแพทยศาสตร์ จุฬาลงกรณ์มหาวิทยาลัย
ปีการศึกษา 2553

VERIFICATION OF IMAGE REGISTRATION FOR THE COMMERCIAL TREATMETN PLANNING SYSTEMS

Miss Sumana Somboon

A Thesis Submitted in Partial Fulfillment of the Requirements
for the Degree of Master of Science Program in Medical Imaging
Department of Radiology
Faculty of Medicine
Chulalongkorn University
Academic Year 2010

Thesis Title	VERIFICATION OF IMAGE REGISTRATION FOR THE COMMERCIAL TREATMENT PLANNING SYSTEMS
By	Miss Sumana Somboon
Field of Study	Medical Imaging
Thesis Advisor	Associate Professor Sivalee Suriyapee, M.Eng.

Accepted by the Faculty of Medicine, Chulalongkorn University in Partial Fulfillment of the Requirements for the Master's Degree

.....Dean of the Faculty of Medicine
(Professor Adisorn Patradul, M.D.)

THESIS COMMITTEE

.....Chairman
(Assistant Professor Chonlakiet Khorprasert, M.D.)

.....Thesis Advisor
(Associate Professor Sivalee Suriyapee, M.Eng.)

.....Examiner
(Associate Professor Tawatchai Chaiwatanarat, M.D.)

.....Examiner
(Associate Professor Kanjana Shotelersuk, M.D.)

.....External Examiner
(Professor Franco Milano, Ph.D.)

สุมนา สมบูรณ์: การตรวจสอบความคลาดเคลื่อนในการซ้อนทับภาพของเครื่องวางแผนการรักษา. (VERIFICATION OF IMAGE REGISTRATION FOR THE COMMERCIAL TREATMENT PLANNING SYSTEMS) อ. ที่ปรึกษาวิทยานิพนธ์หลัก: รศ. ศิวลี สุริยาปี, 52 หน้า.

การซ้อนทับภาพในทางการแพทย์เป็นกระบวนการสำคัญในการวางแผนการรักษาและตรวจสอบความถูกต้องของตำแหน่งการฉายรังสีแบบครอบคลุมเฉพาะก้อนมะเร็ง (conformal radiation) จึงเป็นจุดมุ่งหมายของวิทยานิพนธ์ฉบับนี้ คือ เพื่อศึกษาความถูกต้องของการซ้อนทับภาพด้วย 2 วิธี ของ mutual information และ match point ในเครื่องวางแผนการรักษา 2 เครื่อง คือ เครื่องของ Varian Eclipse V. 8.6.17 และ Oncentra V. 3.2.303 และยังทำการหาวิธีที่เหมาะสมในการซ้อนทับภาพ CT และ Conebeam CT (CBCT) ของผู้ป่วยที่เป็นมะเร็งบริเวณศีรษะและลำคอ จำนวน 20 ราย

การประเมินวิธีการซ้อนทับภาพนี้จะทำในเครื่องวางแผนการรักษา 2 เครื่อง โดยใช้โปรแกรม ImSim QA software กระบวนการเริ่มจาก ImSim สร้างภาพหุ่นจำลองขึ้นมา 3 ชุด โดยชุดแรกเป็นชุดอ้างอิง ชุดที่ 2 ทำการหมุน 5, 10 และ 15 องศา ในแต่ละแนวแกน X, Y, Z และทั้ง 3 แนวแกนพร้อมกัน ส่วนชุดที่ 3 ทำการเลื่อนเป็นระยะ 5, 10 และ 15 มิลลิเมตร ด้วยวิธีเดียวกัน หลังจากนั้นทำการส่งข้อมูลภาพหุ่นจำลองทั้ง 3 ชุดเข้าสู่เครื่องวางแผนการรักษา Eclipse และ Oncentra แล้วทำการซ้อนทับภาพด้วยวิธี mutual information และ match point โดยการซ้อนทับภาพจะกระทำระหว่างภาพอ้างอิง กับภาพที่ได้ทำการหมุนหรือเลื่อนไว้ ความคลาดเคลื่อนในการซ้อนทับจากทั้งสองวิธีจะหาตามวิธีของ Eclipse และ Oncentra หลังจากนั้นภาพบริเวณศีรษะและลำคอของผู้ป่วยที่ได้จากการถ่ายด้วยเครื่อง CT simulator และ CBCT จำนวน 20 ราย จะถูกส่งเข้าเครื่องวางแผนการรักษา Eclipse แล้วทำการซ้อนทับภาพด้วยวิธี mutual information และ match point ระยะการเลื่อนของแต่ละวิธีซ้อนทับภาพจะถูกเปรียบเทียบและประเมินกับระยะเลื่อนโดยรังสีแพทย์บน on-board imager (OBI)

ผลที่ได้จากการซ้อนทับภาพหุ่นจำลองของ ImSim นั้น ความคลาดเคลื่อนของ Eclipse และ Oncentra ใกล้เคียงกัน โดยวิธีการ mutual information ให้ผลการซ้อนทับภาพที่ดีกว่าวิธี match point เนื่องจาก mutual information ใช้ค่าเฉลี่ยความเข้มของทั้งภาพนำมาเข้าคู่กัน แต่ match point ใช้เพียง 4 จุดที่เราเลือกมาเข้าคู่กัน ซึ่งโปรแกรม ImSim สามารถตรวจสอบความแม่นยำของวิธีการได้โดยไม่มีปัจจัยอื่นๆ เช่น การจัดท่าผู้ป่วย หรือการวางหุ่นจำลอง โดยค่าคลาดเคลื่อนจะมากขึ้นเมื่อเราหมุนหุ่นจำลองพร้อมกันทั้ง 3 แนวแกนพร้อมกัน >5 องศา

สำหรับการซ้อนทับภาพของผู้ป่วยนั้น ความคลาดเคลื่อนของแต่ละวิธีเมื่อเปรียบเทียบกับการซ้อนทับภาพโดยรังสีแพทย์นั้น วิธี mutual information และ match point มีค่า 2.02 ± 2.00 มิลลิเมตร, 0.82 ± 1.16 องศา และ3.05 ± 2.92 มิลลิเมตร, 1.31 ± 1.35 องศา ตามลำดับ โดยจะเห็นว่าวิธี mutual information ให้ความคลาดเคลื่อนน้อยกว่าวิธี match point อย่างไรก็ตาม วิธีทั้ง 2 วิธีในการซ้อนทับภาพให้ผลที่น่าเชื่อถือ และสามารถช่วยให้รังสีแพทย์มีความสะดวกและรวดเร็วในการจัดท่าผู้ป่วยก่อนทำการฉายรังสีได้พอๆ กัน

ภาควิชา.....รังสีวิทยา..... ลายมือชื่อนิสิต.....

สาขาวิชา.....ฉายาเวชศาสตร์..... ลายมือชื่อ อ. ที่ปรึกษาวิทยานิพนธ์หลัก.....

ปีการศึกษา.....2553.....

5274830330 : MAJOR MEDICAL IMAGING

KEYWORDS : IMAGE REGISTRATION / IMAGE – GUIDED RADIATION THERAPY (IGRT) / CONEBEAM CT (CBCT) / STATIONARY AND MOVING IMAGE DATASETS

SUMANA SOMBOON: VERIFICATION OF IMAGE REGISTRATION FOR THE COMMERCIAL TREATMENT PLANNING SYSTEMS. THESIS ADVISOR: ASSOC.PROF. SIVALEE SURIYAPEE, 52 pp.

Image registration is essential in treatment planning and position verification for highly radiation conformal delivery methods. The purpose of this study is to evaluate the accuracy of image registration in Varian Eclipse V. 8.6.17 and Oncentra V. 3.2.303 treatment planning system (TPS). Then the suitable image registration method of mutual information and match point between planning computed tomography and cone beam computed tomography are observed for 20 head and neck cases.

The image registration verifications were performed in 2 TPSs using ImSim commercial QA software. The three set of images from ImSim commercial QA software, which the first one was stationary, the second set was 5, 10, 15 degree rotation and the third set was 5, 10, 15 mm translation in X, Y, and Z axes, were imported to Eclipse and Oncentra TPSs. The registration was made between the stationary and moving images. The registration errors were observed for mutual information and match point registration algorithms in each TPS. Then the planning CT image and cone beam CT image for 20 head and neck patients were registered on the Eclipse TPS by the mutual information and match point methods. The position shifts by the two methods were compared and evaluated with those registered optimization by radiation oncologist.

For the registration of ImSim phantom, the Eclipse TPS shows slightly better registration than Oncentra TPS. The mutual information method demonstrates slightly less registration error than match point method, because pixel by pixel is used for mutual information while 4 points is selected for the match point registration method. The ImSim QA software can check both translation and rotation with no influence of setup position compared with the phantom or patient study. The registration error is increased when moving set is rotated >5 degree for all axes.

For cone beam CT registration with planning CT of head and neck patients, the mean deviation from registered optimization by radiation oncologist for mutual information method are 2.02 ± 2.00 mm and 0.82 ± 1.16 degree and for match point method are 3.05 ± 2.92 mm and 1.31 ± 1.35 degree. The mutual information also shows superior image registration than match point method.

From the result the mutual information and match point methods can assist the medical oncologist to optimize the image registration easily and reliably without image misalignment.

Department: .....Radiology..... Student's Signature.....

Field of Study: ....Medical Imaging.... Advisor's Signature.....

Academic Year: .....2010.....

ACKNOWLEDGEMENTS

I would like to deepest appreciate to Associate Professor Sivalee Suriyapee, M.Eng., Division of Radiation Oncology, Department of Radiology, Faculty of Medicine, Chulalongkorn University, advisor, to advise, instruction and support for me. And she also approves English language in this research.

I would like to thank Associate Professor Kanjana Shotelersak, MD., Division of Radiation Oncology and Associate Professor Tawatchai Chaiwatanarat, MD., Division of Nuclear Medicine, Department of Radiology, Faculty of Medicine, Chulalongkorn University, co advisors, for guidance in clinical application.

A special thanks goes to another co advisor, Mr.Sornjarod Oonsiri, M.Sc., Division of Radiation Oncology, King Chulalongkorn Memorial Hospital, for helpful advice in every problem and guide me through this research.

I would like to greatly thank Associate Professor Anchali krisanachinda,Ph.D., Division of Nuclear Medicine, Department of Radiology, Faculty of Medicine, Chulalongkorn University, for teaching of knowledge in Medical Imaging and comments in the research.

I would like to thanks Professor Franco Milano, Ph.D., who were the external examiner of the thesis defense for his help, kind suggestion, and constructive comments in this research.

I would like to thank Mr. Taweap Sanghangthum, M.Sc., Mr.Isra Israngkul-Na-Ayuthaya, M.Sc., Miss Puntiwa Insang, M.Sc. and Miss Chotika Jampangern, M.Sc., and all of the staff at Division of Radiation Oncology, King Chulalongkorn Memorial Hospital, for kindness advice, support and improve English language in this research.

I would like to deeply thank Associate Professor Somjai Wangsuphachart, MD. and Assistant Professor Sukalaya Lerdlum, MD., in Department of Radiology, Faculty of Medicine, Chulalongkorn University for advice and comments in the research.

I would like to thank Mrs. Weeranuch Kitsukjit for her provide suggestion for the improvement.

I am thankful for all teachers, lecturers and staff in the Master of Science Program in Medical Imaging, Faculty of Medicine, Chulalongkorn University for their unlimited teaching of knowledge in Medical Imaging.

Finally, I would like to thank you very much for my family. They always encourage, take care, support in financial and understand me in everything. That's valuable for me.

CONTENTS

Page

Page

LIST OF TABLES

LIST OF FIGURES

Page

LIST OF ABBREVIATIONS

ABBREVIATION	TERMS
2D	Two – dimension
3D	Three – dimension
AEC	Automatic exposure control
aSi:H	Solid-state amorphous silicon
BM	Bone matching
CBCT	Conebeam computed tomography
CCD	Charge-coupled device
cm	Centimeter
CRT	Conformal radiotherapy
CsI	Cesium iodide
CT	Computed tomography
CTV	Clinical tumor volume
DICOM	Digital Imaging and Communications in Medicine
DQE	Detector quantum efficiency
DRRs	Digital reconstructed radiographs
EPIDs	Electronic portal imaging devices
FPD	Flat panel detector
GTV	Gross tumor volume
HNCs	head and neck cancers
HU	Hounsfield unit
ICP	Iterative closest point
IGRT	Image-guided radiation therapy
IM	Image matching
IMRT	Intensity modulated radiotherapy
kV	Kilovoltage
kVp	Kilo-peak voltage
lp/cm	Line pairs per centimeter
mAs	Milliampare second
MDCT	Multidetector computed tomography
mm	Millimeter

ABBREVIATION	TERMS
MRI/MRS	Magnetic resonance imaging, spectroscopy
MTF	Modulation transfer function
MV	Megavoltage
NMI	Normalized mutual information
NPC	Nasopharyngeal carcinoma
OBI	On-board imager
PET	Positron emission tomography
PMMA	Polymethyl methacrylate acrylic
PTV	Planning target volume
QA	Quality assurance
SPECT	Single photon emission computed tomography
TPS	Treatment planning system
US	Ultrasound
VMAT	Volumetric arc therapy

CHAPTER I

INTRODUCTION

1.1 Background and rationale

Treatment of advanced techniques such as 3D conformal, intensity modulated radiotherapy (IMRT) and volumetric arc therapy (VMAT) require accurate delineation of tumor volumes and surrounding healthy tissues for treatment planning, maintained accurate patient setup [1] and compensated for anatomic change during a course of multifraction treatment. Usually, fan beam x-ray computed tomography (FBCT) is the primary imaging modality for structure delineation, beam placement and patient position check. Data from other modalities such as magnetic resonance imaging, magnetic resonance spectroscopy (MRI/MRS) and cone-beam computed tomography (CBCT) can be used to register by combining the specific benefit of each modality together. This is become increasingly necessary for tumor and normal tissue delineation and assessment of patient anatomical change [2]. Image registration is the tool to visualize the anatomical structure clearly and accurately.

The benefit of each imaging modality such as MRI provides superior soft tissue relative to CT and can be used to enhance or suppress different tissues such as fat, the images are shown in Fig.1.1. PET and SPECT can provide unique information about different cellular and physiologic processes to help assess normal and diseased tissues [2]. So the integration of these modalities together can provide better interpretation and decision of doctor to diagnostic or treat the patient, the example is shown in Fig.1.2.

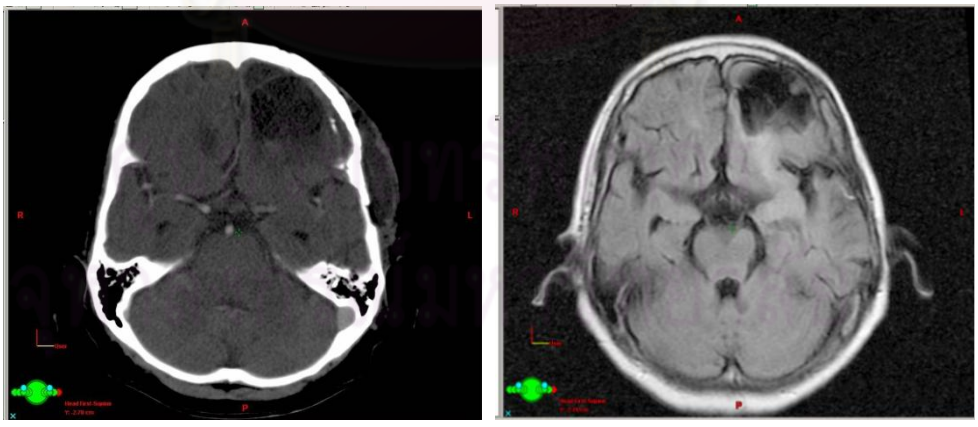

A B

Fig. 1.1, Two types of images A) CT with contrast and B) MRI image datasets.

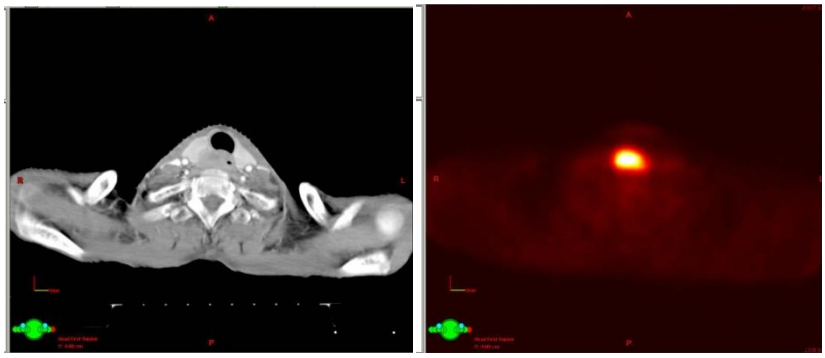

A B

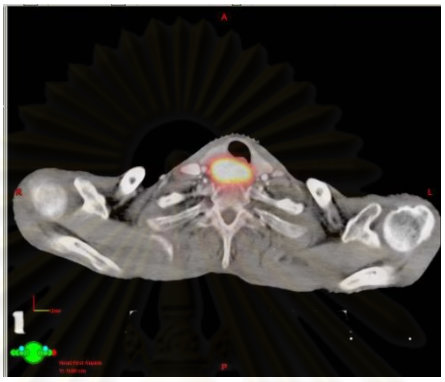

C

Fig. 1.2, Examples of different multimodality imaging data available for treatment planning by A) CT with contrast, B) PET and C) CT with contrast and PET fusion images.

Another application of image registration is to verify the patient position for beam placement before treatment. This process is used to check the position of isocenter that should be at the same position as in the treatment planning process. Kilovoltage cone-beam computerized tomography systems (CBCT) integrated into the gantry of linear accelerator can be employed to acquire high-resolution volumetric images of the patient in the treatment position. The system and image registration are shown in Fig. 1.3.

A B

Fig. 1.3, A) The CBCT system and B) image registration of planning CT and CBCT for patient setup verification.

Image registration is an integrated part of patient management in modern radiotherapy. Image registration is used to find the spatial correspondence between two image datasets acquired at different time. The image registration process is shown in Fig. 1.4. [2]

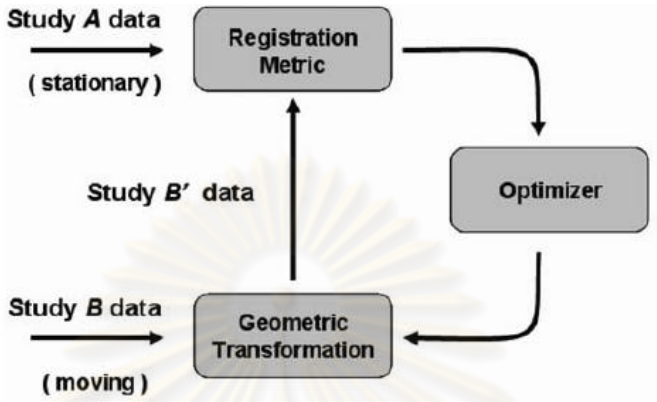

Fig. 1.4, Diagram of image registration process.

The two sets of image, stationary and moving set, are compared. The objective of image registration is to bring the input image into alignment with the base image by applying a optimize transformation parameter to the moving image. Proper registration techniques can improve patient setup, dose delivered and anatomical changes.

The image-guided system (IGRT) with integrated kilovoltage x-ray imaging systems and utilizing CBCT reconstruction techniques could monitor anatomical changes during the course of multifraction radiotherapy treatment, the images are compared against the reference fan beam CT (FBCT) images. Errors in the patient position can be corrected by a couch translation or couch rotation. This leads to the reduction of treatment margin and the reduction of dose in normal tissue. The complication would be less while the tumour control would be increase.

While, the process of image registration between FBCT and CBCT can reduce the uncertainties in delivering dose to the target volume, it is important to evaluate the uncertainties arising from the image registration process. The methods to acquire the image registration errors include the visual inspection, identification of corresponding point landmarks, internal and external fiducial markers.

The purpose of this study is to investigate the accuracy of automatic algorithms provided by two treatment planning systems using Imsim QA software and to validate the suitable image registration method between FBCT and CBCT in head and neck cancer.

1.2 Research objective

1. To determine the accuracy of image registration of two treatment planning by using QA software.

2. To determine the suitable method of image registration to acquire the accurate coordinates in head and neck setup position.

CHAPTER II

REVIEW OF RELATED LITERATURE

2.1 Theories

2.1.1 Head and neck cancer [3]

Radiotherapy, either alone or delivered concurrently with chemotherapy, is a definitive treatment modality for head and neck squamous cell carcinomas. As shown in Fig. 2.1, the volumes that need to be irradiated in head and neck cancers (HNCs) are complex, making it challenging to adequately irradiate the entire targeted volumes while still safely protecting adjacent normal tissues. Many critical structures such as the brain stem, the optic apparatus, and the parotid glands are often located within a few millimeters from the treatment volumes; yet the differences in tumoricidal doses and tolerance doses of the normal structure are often large, demanding a concave dose distribution and steep dose gradients at the tumor boundaries. Conventional two – dimension (2D) radiotherapy and, quite often, three – dimension (3D) conformal radiotherapy (CRT) cannot meet these stringent requirements due to their inability to produce sophisticated dose distributions, resulting in reluctant compromise between adequate tumor coverage and protection of sensitive structures. Advancement of computer optimization and intensity – modulated radiation therapy (IMRT) significantly improved the conformity of the dose distributions as well as the gradient of dose fall – off.

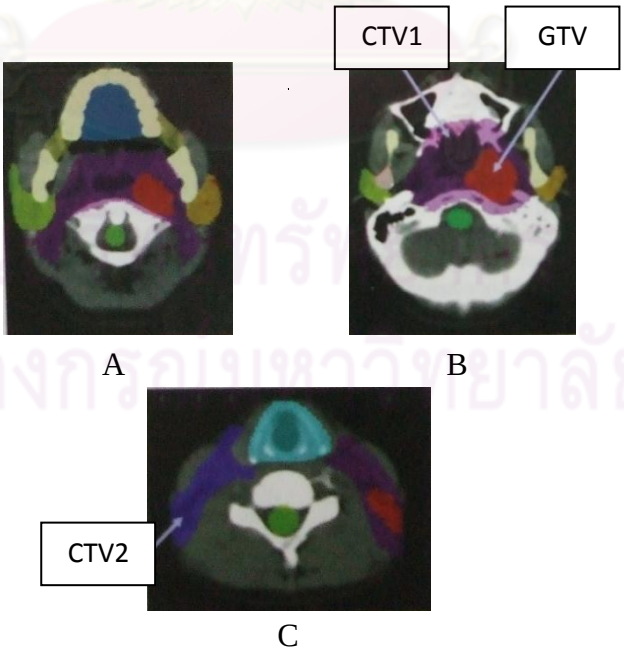

Fig. 2.1, A) Illustration of complex tumor volumes in relationship with numerous normal organs in vicinity. B) The tumor volumes include the gross tumor volume (GTV), high- risk clinical tumor volume (CTV1), and C) low-risk clinical tumor volume (CTV2).

Although early clinical results of 3D – CRT and IMRT for patients with HNCs are promising, uncertainties in the radiation delivery of these sophisticated plans become a great concern. In particular, the question of whether these highly conformal dose distributions can be precisely delivered to the patients over a protracted course of 6 to 7 weeks of treatment becomes paramount. Specifically, can we safely reduce the planning margins while patient positioning uncertainties persist? Can these problems be solved with implementation of image guidance? What kind of image guidance is optimal in these patients? To answer these questions, imaging guidance in radiation management of HNC patient is applied.

2.1.2 Image-guided radiation therapy (IGRT) [4]

Radiation therapy is a local treatment that is designed to treat the defined tumor and spare the surrounding normal tissue from receiving doses above specified dose tolerances. There are many factors that may contribute to differences between the planned dose distribution and the delivered dose distribution. One such factor is uncertainty in patient position on the treatment unit. IGRT is a component of the radiation therapy process that incorporates imaging coordinates from the treatment plan to be delivered in order to ensure the patient is properly aligned in the treatment room.

Image-guided radiation therapy (IGRT) is the process of frequent two and three-dimensional imaging, during a course of radiation treatment, used to direct radiation therapy utilizing the imaging coordinates of the actual radiation treatment plan. The patient is localized in the treatment room in the same position as planned from the reference imaging dataset. An example of imaging for treatment guidance which is used today are:

2.1.2.1 Portal imaging [5]

Portal imaging has progressed from the use of film as the imaging detector, through screen/camera imagers and liquid ionization chambers, to solid-state flat-panel detectors. Although there are institutions still equipped with and using the older detector systems, the flat-panel imager is emerging as the new standard detector for portal imaging in IGRT.

2.1.2.2 The electronic portal imaging device (EPID) [6]

EPID is a relatively new development in portal imaging. It consists of an image acquisition unit fitted to the linear accelerator (Linac), and a component that digitizes and displays these images on a computer screen. The unit should provide high resolution and high contrast images, to allow rapid verification of treatment field shape and position immediately after the patient's X-ray exposure. Recent developments include the software to analyze portal images and compare them with treatment planning images for setup accuracy and localization.

2.1.2.3 Ultrasound (US)

In ultrasound, a signal generator is combined with a transducer. Piezoelectric crystals in the signal generator convert electricity into high-frequency sound waves, which are sent into tissues. The tissues scatter, reflect, and absorb the sound waves to various degrees. The sound waves that are reflected back (echoes) are converted into electric signals. A computer analyzes the signals and displays the information on a screen. [7]

Ultrasound (US) is one method of performing IGRT for prostate cancer, and several devices are commercially available for this purpose. Most US-IGRT systems operate by comparing US images obtained at time of treatment to X-ray computed tomography (CT) images obtained at time of planning so as to measure daily prostate misalignments. However, this "cross-modality" comparison approach has inherent difficulties (in part because the prostate base is frequently difficult to visualize on CT), and discrepancies between US and other IGRT approaches have been reported.

A new system offers an alternative by incorporating an US system in the CT simulation room in addition to the US system in the treatment room. This second US system is used to acquire an US reference scan at the time of planning and allows for an intramodality comparison of planned and treatment images. In both rooms, an infrared imaging system that tracks the position of the US probe is used to relate the US scans to the room coordinates and to the machine isocenter. This ceiling-mounted camera system is located at the foot of each treatment couch. Recent results indicate that this intramodality approach provides more accurate measures of prostate misalignment than does the conventional cross-modality approach. [8]

2.1.2.4 Computed Tomography (CT)

The introduction of computed tomography (CT) in clinical practice resulted in high quality 3D images, which allowed precise definition of tumor shape and location. This information motivated technology development, which would allow planning and delivery of radiation in a more conformal way aiming to give enough dose for disease elimination while sparing healthy tissues[9]. In-room CT planar radiography is useful for setup guided by either bony landmarks or implanted fiducials but is of limited use in assessing soft tissue position and shape. In-room CT has been developed to assist soft-tissue target alignment before the start of treatment. In one approach a conventional CT scanner is placed in the treatment room on the same couch axis as the LINAC gantry. Another approach uses a kV source and diagnostic detector mounted to the treatment gantry at 90^{o} with respect to the LINAC [5].

2.1.2.5 Conebeam computed tomography (CBCT) [10]

Conebeam x-ray CT (CBCT) is a developing imaging technique designed to provide relatively low-dose high-spatial-resolution visualization of high-contrast structures in the head and neck and other anatomic areas.

Conebeam x-ray CT (CBCT) is a relatively recent installment in the growing inventory of clinical CT technologies. The first prototype clinical CBCT scanner was adapted for angiographic applications in 1982. The arrival of marketable scanners in the last 10 years has been, in part, facilitated by parallel advancements in flat panel detector (FPD) technology, improved computing power, and the relatively low power requirements of the x-ray tubes used in CBCT. These advancements have allowed CBCT scanners to be sufficiently inexpensive and compact for operation in office-based head and neck as well as dental imaging applications. These systems are distinguished by a conical x-ray beam geometry and the use of 3D reconstruction algorithms; most recent models are also fit with FPDs. For the fundamental of CBCT is described in the topic below:

2.1.3. Fundamental principles of CT and CBCT

Although there are numerous differences between CBCT and conventional fan-beam CT techniques, many of the fundamental physical concepts are the same.

2.1.3.1 Fundamental principles of CT [10]

The original clinical CT scanner was introduced by Sir Godfrey N. Hounsfield in 1967. Data acquisition was based on a translate-rotate parallel-beam geometry wherein pencil beams of x-rays were directed at a detector opposite the source and the transmitted intensity of photons incident on the detector was measured. The gantry would then both translate and rotate to capture x-ray attenuation data systematically from multiple points and angles. Although x-ray sources, acquisition geometries, and detectors have rapidly evolved since Hounsfield's original scanner, the theory behind CT has not changed.

The attenuation of a monochromatic x-ray beam through a homogeneous object is described by the Lambert-Beer law:

$$I = I_0 e^{-\mu x}$$

Where I is the transmitted photon intensity, I_o is the original intensity, x is the length of the x-ray path through the object, and μ is the linear attenuation coefficient of the material traversed. This expression changes for inhomogeneous materials such as human tissue:

$$I = I_0 e^{-\int \mu x \, dx}$$

Line integrals of the linear attenuation coefficients, μ, can be obtained by taking the negative logarithm of the above expression. A line integral at angle θ through the object is the ray sum, a set of which at a given θ constitutes a

projection. The computational problem in CT is to determine μ at a given point from a large set of projections obtained at varying θ about the object, a computation based on the theory formulated by Radon in 1917.

Data acquisition in conventional CT imaging has evolved through 4 generations of acquisition geometries. First-generation scanners used parallel pencil beams of x-rays and required both translation and rotation of the source and a single-detector apparatus. Second-generation scanners introduced fan-beam x-ray geometry and used a single-detector linear array. In third-generation scanners, the single-detector arc was introduced in conjunction with fan-beam x-ray geometry. Fourth-generation scanners used a fan-beam of x-rays and a circular detector array. In current practice, multidetector helical CT (MDCT) scanning is most frequently used, answering the call for reduced acquisition times. MDCT is loosely based on third-generation geometry, though the detector array has multiple rows of detectors.

2.1.3.2 Data acquisition of CBCT [10]

In CBCT systems, the x-ray beam forms a conical geometry between the source (apex) and the detector (base) (Fig 2.1). This is in contrast to conventional fan-beam geometry, in which the collimator restricts the x-ray beam to approximately 2D geometry. In a fan-beam single-detector arc geometry, data acquisition requires both rotation and z-direction translation of the gantry to eventually construct an image set composed of multiple axial sections. In CBCT systems using a 2D FPD, however, an entire volumetric dataset can be acquired with a single rotation of the gantry. Incident photons on multiple-row detectors in MDCT actually fall on a 2D area of detectors, as with flat-panel detection; indeed, with increasing numbers of rows in MDCT detector arrays, the acquisition geometry actually approximates that of a conebeam system.

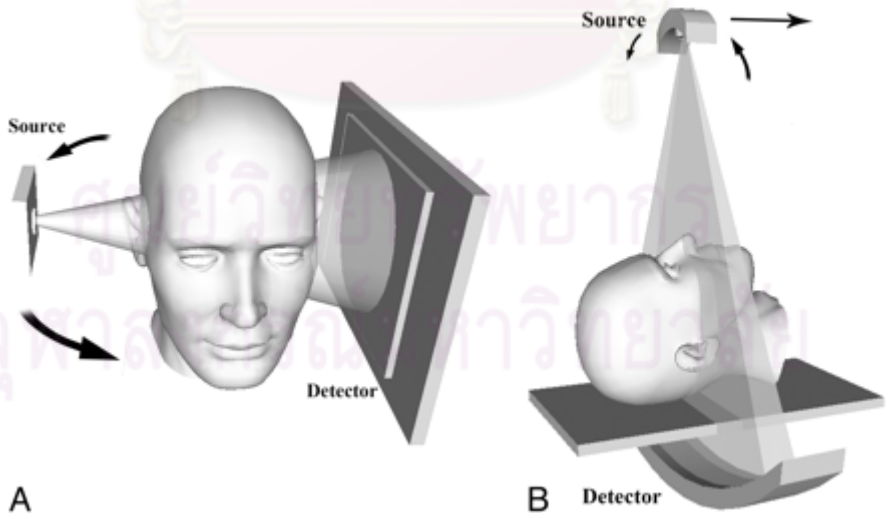

Fig. 2.2, Depiction of CT acquisition geometries. A) Conebeam geometry in a compact office-based system designed for the patient to sit upright. B) Conventional fan-beam geometry as it is used in MDCT scanners with the patient supine.

2.1.3.3 Flat panel detectors (FPDs) [10]

Digital FPDs enable the direct conversion of x-ray energy into a digital signal with high spatial resolution. The fundamental design consists of a screen of scintillator crystals grown onto a matrix of photodiodes embedded in a solid-state amorphous silicon (aSi:H) or selenium layer. Incident x-rays are photochemically converted to light by the scintillator film and transmitted directly to the photodiode array where the signal-intensity charge is stored. Thin-film transistors fabricated into the aSi:H matrix relay a signal intensity proportional to the stored charge in the photodiode array, which is, in turn, proportional to the incident photons on the scintillator layer. The FPD used in the MiniCAT is an indirect-conversion system based on a cesium iodide (CsI) scintillator embedded in an aSi:H layer. CsI scintillators produce superior spatial resolution owing to the microscopic columnar structure of the CsI substrate, which serves essentially as a fiber-optic conductor for the signal intensity being transmitted to the photodiode array. FPD arrays afford greater spatial resolving potential with similar noise intensity when compared with their x-ray intensifier/charge-coupled device (CCD) predecessors.

2.1.4 Image quality of CBCT [10]

Several physical descriptors and parameters are commonly enlisted to characterize the quality of an image. In characterizing CT systems, quantum noise, spatial resolution, contrast resolution, and detector quantum efficiency (DQE) are of particular interest. Quantum noise is fundamentally related to image quality and is a function of dose, tissue transmissivity, and voxel size. Noise is, in turn, a principal determinant of contrast resolution and, to a lesser extent, spatial resolution, which, along with artifacts, constitute the major observable determinants of overall image quality. CBCT imaging with FPD technology typically affords excellent spatial resolution with a relatively low patient dose. Contrast resolution suffers, however, due to increased x-ray scatter and the reduced temporal resolution and dynamic range of the FPDs. Scatter will be addressed in detail due to its particular impact on contrast resolution. Dynamic range and temporal resolution will also be addressed in addition to several proposed approaches to improvements in CBCT image quality.

2.1.4.1 Spatial resolution [10]

The spatial resolution of an imaging system is its ability to discriminate objects of different attenuation at small separation distances. It is typically described as the spatial frequency (measured in line pairs per centimeter [lp/cm]) that can be discriminated with a 10% detection of true contrast. The "modulation transfer function" (MTF) relates the percentage of actual contrast conferred to the spatial frequency of inserts in a phantom and is the product of the Fourier transform of a composite of functions describing image blur, unsharpness, and contrast response in reference to the ability to resolve line pairs per unit length. Spatial resolution is determined primarily by the inherent blurring in the detection apparatus and the

individual area of the detection elements. Superior spatial resolution is one of the most attractive qualities of CBCT imaging and is largely the result of FPD technology and isotropic data acquisition.

2.1.4.2 Low-contrast detectability [10]

Contrast resolution describes the ability of an imaging system to discriminate differences in tissue attenuation, as measured in HU. The low-contrast detectability in CBCT systems depends on both the dynamic range and temporal resolution of the detector as well as x-ray scatter and quantum noise.

CBCT systems under evaluation for head and neck imaging are typically described as having soft-tissue contrast discrimination of approximately 10 HU. Modern MDCT scanners have contrast resolution approaching 1 HU. This limited contrast resolution remains a barrier to the extension of CBCT technologies into diagnostic imaging, in which detection of small changes in soft-tissue attenuation is a premium. Recent research has focused on scatter reduction and improvements in dynamic range and temporal resolution in an effort to improve contrast resolution without unnecessarily increasing patient dose. In fact, 3-HU discrimination has been achieved in experimental CBCT systems, though this has yet to translate to commercial scanners.

2.1.5 Image registration [11]

Image registration is the process of transforming different sets of data into one coordinate system. Data may be multiple photographs, data from different sensors, from different times, or from different viewpoints. It is used in computer vision, medical imaging, military automatic target recognition, and compiling and analyzing images and data from satellites. Registration is necessary in order to be able to compare or integrate the data obtained from these different measurements. In this study, the rigid body model is used to registering with registration methods. The rigid body model is discussed below:

2.1.5.1 Rigid body model [12]

For medical imaging, the most constrained spatial transformation model is the rigid body model. This model asserts that distances and internal angles within the images cannot be changed during registration. As the name implies, this model assumes that the object behaves in the real world as a rigid body, susceptible to global rotations and translations, but internally immutable. This model is well suited to object such as individual bones, which cannot be deformed. To a reasonable approximation, this model is also applicable to the brain, which is encased in bones that protect it from forces that might lead to deformations. However, it is well established that this is only an approximation, since parts of the brain, such as the brainstem, are subject to distortions induced by cardiac and respiratory cycles. For

images accumulated over many cardiac and respiratory cycles, these movements may result in a blurred but highly consistent signal that follows the rigid body assumptions quite well. However, for images acquired with a very short time frame, these movements can produce very clear violations of the rigid body model assumptions.

Medical images often consist of voxels that differ in the real world distances that they represent along the X, Y and Z axes. For example, it is common for the slice thickness in magnetic resonance imaging data to be larger than the size of individual pixels within each slice. If ignored, these anisotropies in voxel size will clearly lead to apparent violations of the rigid body model, even for solid structures that accurately follow the rigid body assumptions in the real world. Consequently, any implementation of a rigid body model must explicitly correct for voxel sizes to ensure that the real world distances and angles that are being represented do not change. In a worst case scenario, six different voxel sizes may be involved: three anisotropic voxel sizes from one image, and three different anisotropic voxel sizes from the other image. A properly implemented rigid body model for transforming such images may choose any one of these voxel sizes or may even select some other arbitrary voxel size. However, calculations must be included to rescale distances to compensate for the various voxel sizes. For the rigid body model to be applicable, all six of the voxel sizes must be known accurately. If the voxel sizes are not known with certainty, the best strategy is to scan a phantom with known dimensions to determine the true voxel dimensions since errors in specification of the voxel dimensions will lead to unnecessary errors in registrations produced using a rigid body model. If this is not possible, the calibration error can be estimated by adding additional parameters to augment the rigid body model.

In three dimensions, the rigid body model requires specification of six independent parameters. It is traditional (but not necessary) for three of these parameters to specify a three dimensional translation that is either preceded or followed by the sequential application of specified rotations around each of the three primary coordinate axes. However, before considering the three dimensional model, it is useful to consider the simpler case of two dimensions. In two dimensions, the rigid body model requires only three independent parameters.

For this research, the Landmark-based registration method and Intensity-based registration method were used, they are described below:

2.1.5.2 Landmark-based registration methods [11]

Landmarks can be anatomical, i.e. salient and accurately locatable points of the morphology of the visible anatomy, usually identified interactively by the user. Technically, the identification of landmark points is a segmentation procedure, but we reserve the classification segmentation-based registration for methods relating to segmentation of structures of higher order, i.e. curves, surfaces and volumes. Landmark-based registration is versatile in the sense that it, at least in theory, can be applied to any image, no matter what the object or subject is. Landmark-based

methods are mostly used to find rigid or affine transformations. If the sets of points are large enough, they can theoretically be used for more complex transformations. Anatomical landmarks are also often used in combination with an entirely different registration basis methods that rely on optimization of a parameter space that is not (nearly) convex are prone to sometimes getting stuck in local optima, possibly resulting in a large mismatch. By constraining the search space according to anatomical landmarks, such mismatches are unlikely to occur. Moreover, the search procedure can be sped up considerably. A drawback is that user interaction is usually required for the identification of the landmarks. In landmark-based registration, the set of identified points is sparse compared with the original image content, which makes for relatively fast optimization procedures. Such algorithms optimize measures such as the average distance between each landmark and its closest counterpart, or iterated minimal landmark distances. For the optimization of the latter measure the iterative closest point (ICP) algorithm and derived methods are popular. Its popularity can be accredited to its versatility (it can be used for point sets, and implicitly and explicitly defined curves, surfaces and volumes), computational speed and ease of implementation. The Procrustean optimum can sometimes be computed, but is more commonly searched for using general optimization techniques. Yet other methods perform landmark registration by testing a number of likely transformation hypotheses, which can, for example, be formulated by aligning three randomly picked points from each point set involved. Common optimization methods here are quasi-exhaustive searches, graph matching and dynamic programming approaches.

2.1.5.3 Mutual information-based methods [2]

For data from different modalities where the pixel intensities of corresponding anatomy are typically (and inherently) different, registration metrics based on simple differences or products of intensities are not effective. In these cases, sophisticated metrics based on intensity statistics are more appropriate. When using these metrics, there is no dependence on the absolute intensity values. One such metric that has proved very effective for registering image data from different modalities is called mutual information (MI). As the name implies, this metric is based on the information content of the two imaging studies and is computed directly from the intensity distributions of the studies.

According to information theory, the information content H of a “signal” is measured by the expectation (of the log) of the probability distribution function (PDF) of the signal values. For image data, the signal values are the gray-scale intensities and the PDF is the normalized histogram of these intensities. The information content in the image data is

$$H(I_A) = -E[log_2\, p(I_A)] = -\sum p(I_A)\, log_2\, p(I_A),$$

Where $p(I_A)$ is the probability distribution function of the intensities I_A of Study A (Fig. 2.3).

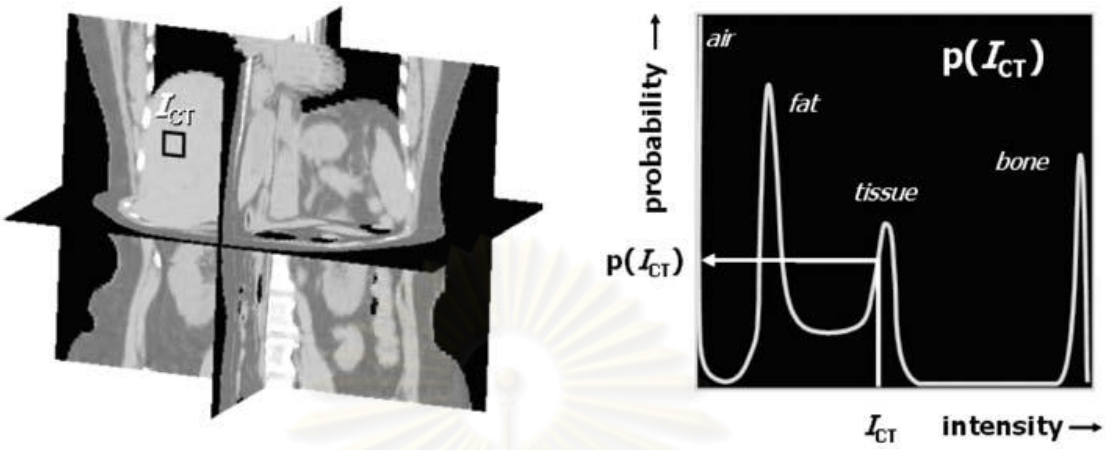

A B

Fig. 2.3, A) 3D image volume B) probability density function of the image intensiteis

The joint or combined information content of two imaging studies has the same form and represents the information content of the two studies fused together. This is computed as

$$H(I_A, I_B) = -\sum\sum p(I_A, I_B)\, log_2\, p(I_A, I_B),$$

Where $p(I_A, I_B)$ is the 2D joint probability distribution function of the intensities I_A of Study A and I_B of Study B (Fig. 2.4). This PDF is constructed from the pairs of gray-scale values at each common point in Study A and Study B.

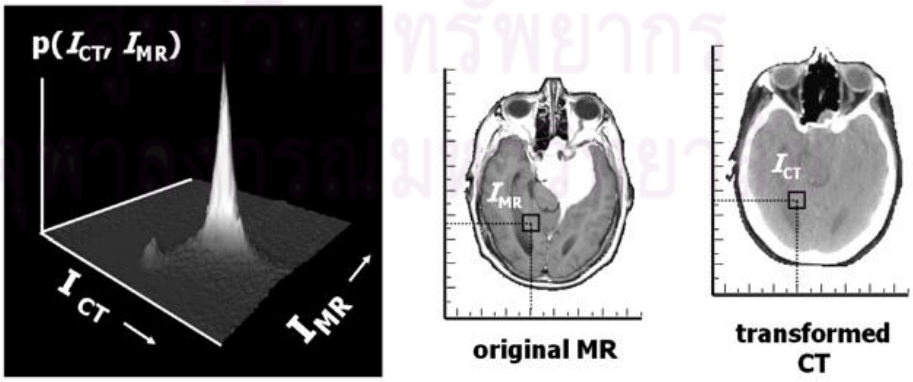

A B C

Fig. 2.4, A) Two-dimensional joint-intensity histogram constructed from B) an MR scan (Study A) and C) a transformed (reformatted) CT (Study B)

The joint or total information content for the two imaging studies is always less than or equal to the sum of the individual information contents:

$$H(I_A, I_B) \leq H(I_A) + H(I_B),$$

If there is no redundant information in the pair of imaging studies (e.g., they are completely independent), the joint information of the pair is simply the sum of the information in Study A and Study B:

$$H(I_A, I_B) = H(I_A) + H(I_B),$$

If there is some redundant information, then the joint information content will be less than the sum of the information in the two studies:

$$H(I_A, I_B) < H(I_A) + H(I_B),$$

The amount of shared or mutual information is just the difference between the sum of the individual information contents and the joint information content,

$$MI(I_A, I_B) = H(I_A) + H(I_B) - H(I_A, I_B),$$

Solving for MI from the above equations,

$$MI(I_A, I_B) = \sum\sum p(I_A, I_B)\, log_2\, [p(I_A, I_B)/p(I_A)p(I_B)],$$

The mutual information between two imaging studies can be thought of as the information in Study B that is also present in Study A. Accordingly, one way to describe mutual information is as the amount of information in Study B that can be determined (or predicted) from Study A. To completely predict Study B from Study A, each intensity value in Study A must correspond to exactly one intensity value in Study. When this is the case the joint intensity histogram has the same distribution as the histogram of Study A, and $H(I_A, I_B)$ equals $H(I_A)$. The MI is therefore equal to $H(I_B)$, and Sutdy B at this point can be thought of as a "recolored" version of Study A.

A major advantage of mutual information is that it is robust to missing or incomplete information. For example, a tumor might show up clearly on an MR study but be indistinct on a corresponding CT study. Over the tumor volume the mutual information is low, but no prohibitive penalties are incurred. In the surrounding healthy tissue the mutual information can be high, and this becomes the dominant factor in the registration.

2.1.6 Validation of registration accuracy

There are many techniques to assess image registration error, often employed in combination. These include (a) visual inspection, (b) identification of corresponding point landmarks, (c) internal and external fiducial markers, (d) comparison with previously validated methods, (e) use of virtual and physical phantom, (f) misalignment of images by artificial transformation of images either randomly or systematically sampling the parameter space and (g) consistency using three images [14]. The example of some techniques was discussed below.

2.1.6.1 Visual inspection [12]

One of the quickest validation methods to implement is simple visual inspection of the result. Although this may seem like and informal and potentially unreliable approach, some research have shown that visual inspection can detect 2 mm misregistrations of brain MRI images to brain CT images quite reliably. Misregistration can be accurately identified even when one of the images is a low-resolution PET image. In general, if the images look misregistered, they probably are misregistered, and visual inspection should be used as a routine ongoing validation approach at every opportunity.

2.1.6.2 Use of virtual and physical phantom [12]

In the absence of gold standards, simulations are sometimes used to estimate registration accuracy. A common strategy is to take real data and deform it using an appropriate spatial transformation model while simulating the addition of noise and other factors thought to be relevant in limiting registration accuracy. Simulations are most useful when addressing the question of how sensitive a registration method is to some particular aspect of the data. For example, simulations might be very helpful when trying to choose the optimum amount of smoothing that should be applied to images for intensity based intramodality registration. The results of such simulations can serve a very important role in optimizing the performance of a registration method. However, in the context of validation, simulations have definite limitations that can make them overestimate or underestimate registration accuracy. Simulations are especially poor in the context of comparing different methods to one another. The limitations of simulations derive from the fact that they are based on models of reality and not on reality itself. These models may omit factors that limit registration accuracy in the real world, or they may overestimate the degree to which a limiting factor is actually present. The models used to create simulated data for registration necessarily include spatial transformation models, interpolation models, and models of noise. Registration methods typically also implement spatial transformation models, interpolation models, and noise models either explicitly or implicitly. If the two sets of models are congruent, but this provides little assurance that actual performance will be as good. To the extent that the models are not congruent, any

poor performance will be difficult to evaluate since it can be blamed on the discrepancy between models.

2.2 Review of related literature

Wang X et al. [15] evaluated the accuracy and efficiency of 3 image registration algorithms for CT and MRI fusion by using 12 sets of CT and MRI scans in 12 nasopharyngeal carcinoma (NPC) patients. Three algorithms of registration which were Mark-and-link, Interactive, and Normalized mutual information (NMI) were evaluated by performing statistical analysis of the coordinate difference between CT and MR anatomical landmarks along the x, y, and z axes. The time required to complete the registration process using three algorithms was also recorded to evaluate the efficiency of each image registration. The result is shown in Table 2.1 and Table 2.2.

Table 2.1, The registration errors for 3 image registration algorithms.

	X (mm)	Y (mm)	Z (mm)
Mark-and-link	0.66	1.03	0.58
Interactive	0.70	1.04	0.64
Normalized mutual information (NMI)	0.68	1.03	0.56

Table 2.2, Mean time required for CT/MRI registration.

Algorithms	Time (min)
Mark-and-link	6.25
Interactive	5.25
Normalized mutual information (NMI)	5.15

From this result, all three registration algorithms, mark-and-link, interactive, and NMI, could provide accurate CT/MRI registration. However the mark-and-link method was most time consuming.

Plaquin N. and Rangel A. [1] used phantom to evaluate a commercially available three modality image guided radiation therapy system (IGRT) which consist of megavoltage (MV) planar, kilovoltage (kV) planar and conebeam CT imaging system. The registration was performed between appropriate digitally reconstructed radiographs (DRRs) of pelvic phantom from conventional CT scan and three modality of IGRT image dataset. Seventeen controlled displacements of the couch from the reference position were made for the MV, kV, and CBCT images. Of these 17 displacements, 12 accurate displacements were made in each of the three orthogonal directions independently and the remaining 5 were combinations of all three directions. The three registration methods, automatic image registration, semiautomatic registration and manual registration, was performed by Varian equipment.

All imaging modalities used three image registration have average residual translation setup error less than 1 mm by kV planar imaging and automatic image registration were found to give the highest accuracy and precision overall.

Buhl SK, Duun-Christensen AK, Kristensen BH, Behrens CF. [16] performed the Clinical evaluation of 3D/3D MRI-CBCT automatching on brain tumors for online patient setup verification. Initially, a multi-modality phantom was constructed and used for a quantitative comparison of CT-CBCT and MRI-CBCT automatching. Following the phantom experiment, three patients undergoing postoperative radiotherapy for malignant brain tumors received a weekly CBCT. In total 18 scans was matched with both CT and MRI as reference. The CBCT scans were acquired using a Clinac iX 2300 linear accelerator (Varian Medical Systems) with an On-Board Imager (OBI).

The phantom experiment on CT-CBCT and MRI-CBCT automatching obtained similar results. A significant difference was observed only in the longitudinal direction where MRI-CBCT resulted in the best match (mean and standard deviations of 1.85±2.68 mm for CT and -0.05±2.55 mm for MRI). For the clinical experiment, the absolute difference in couch shift coordinates acquired from MRI-CBCT and CT-CBCT automatching, were ≤2 mm in the vertical direction and ≤3 mm in the longitudinal and lateral directions. For yaw rotation differences up to 3.3 degrees were observed. Mean values and standard deviations were 0.8±0.6 mm, 1.5±1.2 mm and 1.2±1.2 mm for the vertical, longitudinal and lateral directions, respectively and 1.95±1.12 degrees for the rotation (n=17).

From the result, it is feasible to use MRI as reference when conducting 3D/3D CBCT automatching for online patient setup verification.

Fox T., Huntzinger C., Hohnstone P., Ogunleye T. and Elder E. [17] evaluated the performance of the image registration software for automatically and repositioning by 3D offset of a phantom using kilovoltage onboard imaging (OBI) system. The geometric rigid phantom and anthropomorphic head phantom containing a humanoid skeleton were used to assess the precision and accuracy of the automated positioning system. The geometric phantom translation offset of 3 mm, 5 mm and 9 mm were performed and anthropomorphic phantom offset were 5 mm, 10 mm and 15 mm. Test was also performed with combined shifts in the three principal directions with the phantom offset by 5 mm to 10 mm simultaneously. Then the couch rotation was performed with 2 and 5 degree. The final performed were combined translation and rotation of phantom.

From the translation only, average magnitude of displacement was less than 0.75 mm for each of three principal directions. Combine translation and rotations had the greatest average deviation in lateral, longitudinal and vertical direction. For all dimensions, the magnitude of the deviation does not appear to be correlated with the magnitude of the actual translation introduced.

From this result, the OBI system has been successfully integrated into a feasible online radiotherapy treatment guidance procedure. Evaluation of each

patient's resulting automatch should be performed by therapists before each treatment session for adequate clinical oversight

Ryan et al. [18] quantified prostate misplacement that result from automatic bone matching (BM) and image matching (IM) registration algorithms. 204 megavoltage CT (MVCT) images and planning CT from 8 high-risk tomotherapy prostate patients were incorporated into this study. Daily prostate misplacement was determined by calculating from BM and IM algorithms.

Mean and maximum 3D prostate positioning errors were 3.7 ± 2.1 mm and 11.8 mm for bone matching and 4.6 ± 2.3 mm and 11.5 mm for image matching, respectively.

From this study, it is suggested that the image registration should be used for bone matching instead of image matching for tomotherapy prostate patients.

CHAPTER III

RESEARCH METHODOLOGY

3.1 Research design

This study is an observational descriptive study research.

3.2 Research design model

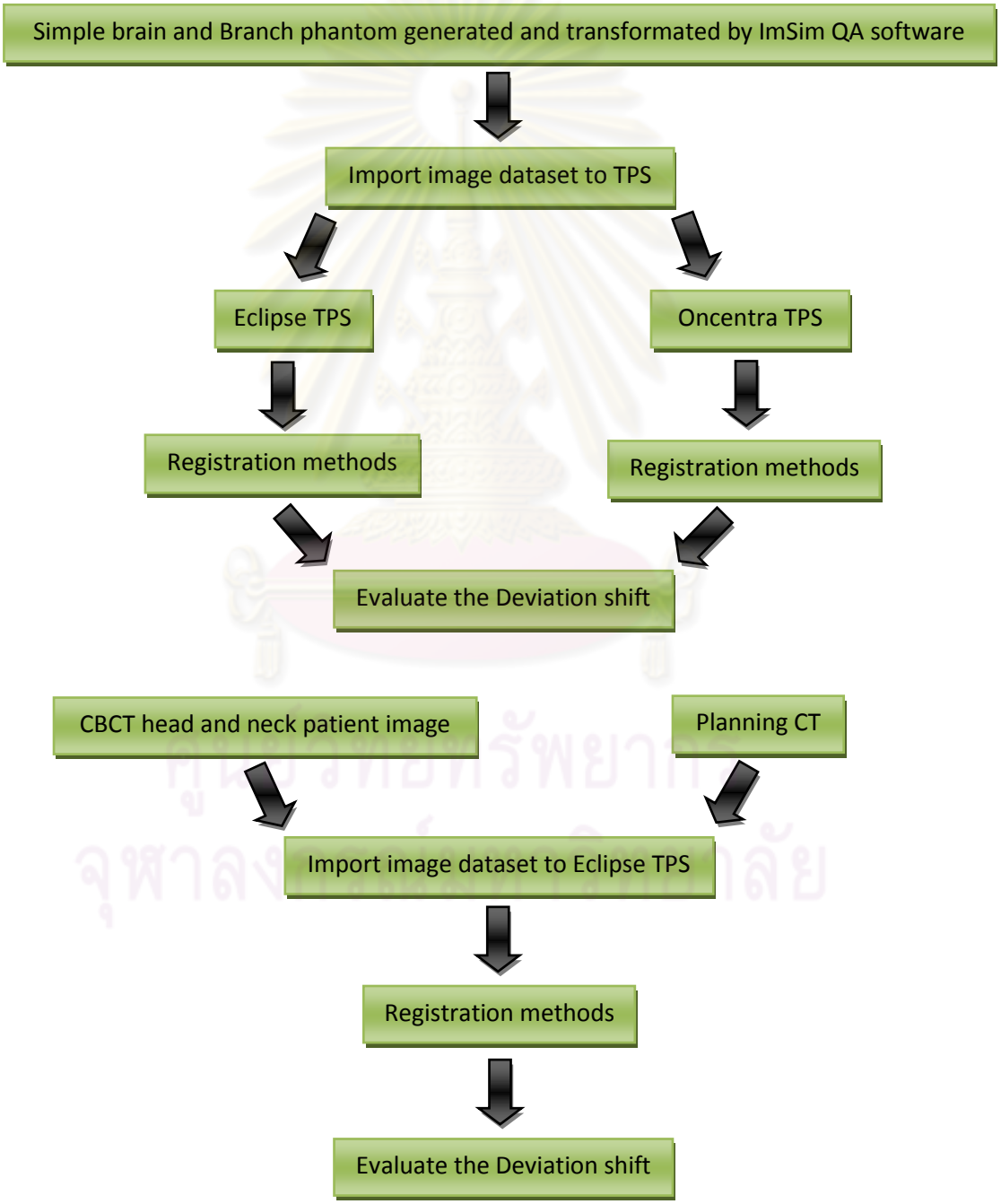

Fig 3.1, Research design model.

3.3 Conceptual frameworks

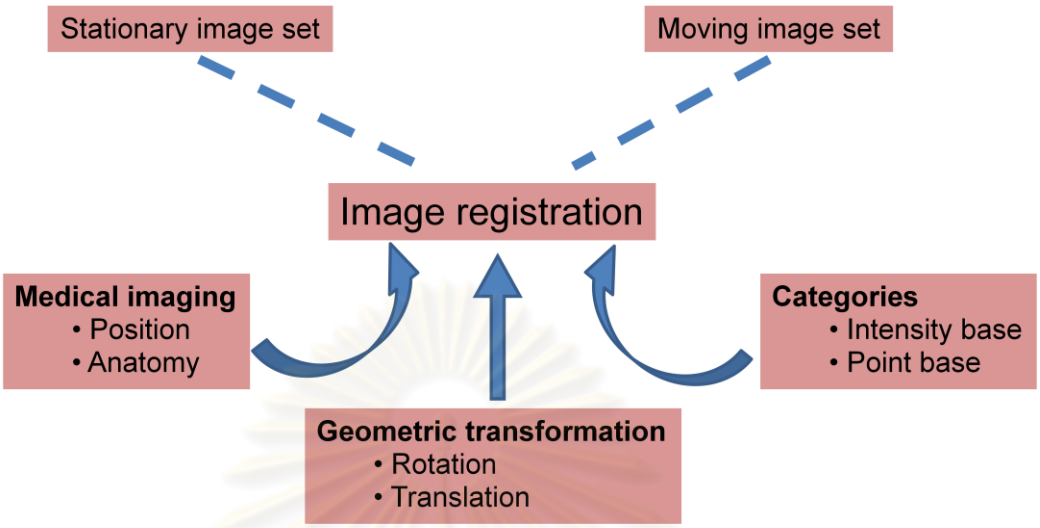

Fig. 3.2, Conceptual frameworks.

3.4 Key word

- Image registration
- Image-guided radiation therapy (IGRT)
- Conebeam CT (CBCT)
- Stationary and moving image datasets

3.5 Research questions

3.5.1 Primary question

How accurate of the image registration for two treatment planning systems?

3.5.2 Secondary question

What is the most suitable method of registration between planning CT and conebeam CT in head and neck region?

3.6 Materials

3.6.1 ImSim QA software

ImSim QA software (Modus Medical Devices Inc., North Routledge Park London ON N6H 5L6, Canada), which is shown in Fig. 3.3, is the software designed to aid the physicist testing a range of medical imaging and radiotherapy applications such as rigid and elastic image fusion algorithms, IGRT and 4D imaging systems. It is ideal for training in image fusion, auto segmentation, 3D margin growing and CT/MR/PET imaging.

ImSim QA provides a toolkit of 15 virtual phantoms that can be extensively edited and transformed, before being converted to DICOM CT, MR & PET simulated images. With the ability to add noise, change density, change slice spacing and re-orientate, the phantom DICOM images are then exported to the test application, minimizing the use of the real scanner and increasing the efficiency of testing. Real DICOM images can also be imported into ImSimQA for editing, without having to re-scan.

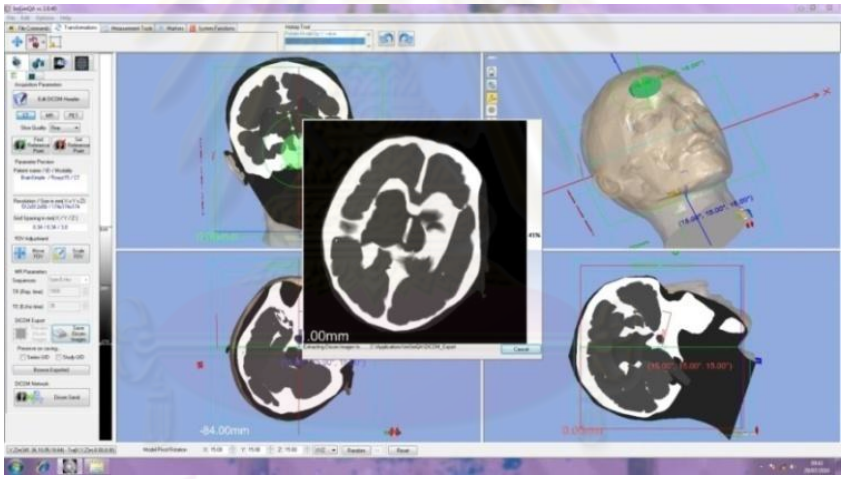

Fig. 3.3, ImSim QA software.

3.6.2 Treatment planning system

a. Eclipse treatment planning system

Eclipse treatment planning version 8.6.17 (Varian Medical System, Palo Alto, CF, USA) is a treatment planning for all modalities such as 3D conformal, IMRT, electron, proton, and brachytherapy. Eclipse helps dosimetrists, physicists, and physicians efficiently create, select, and verify the best treatment plans for their patients. The configuration of Eclipse TPS is shown in Fig. 3.4

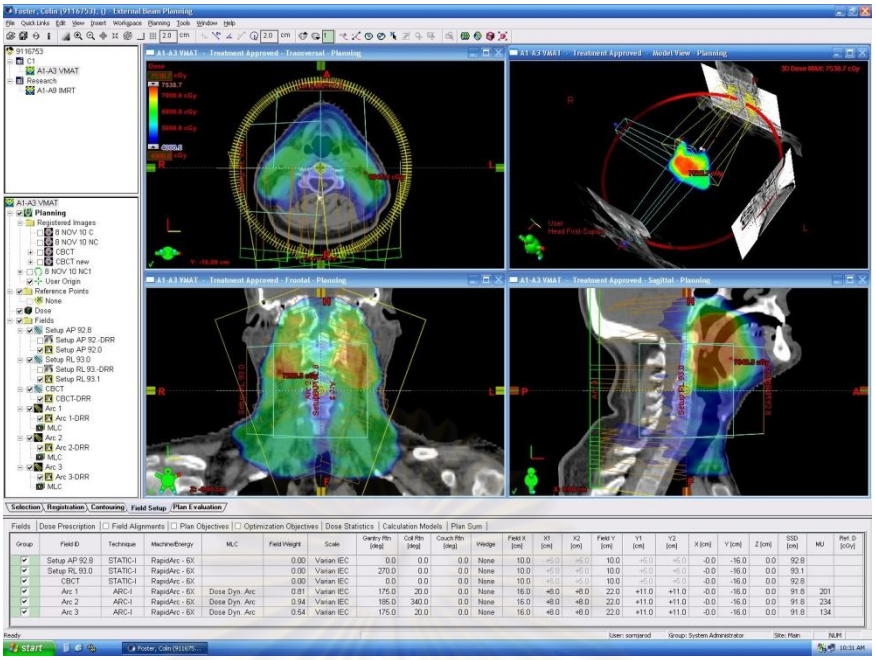

Fig. 3.4, Eclipse treatment planning system showing 3D dose distribution.

b. Oncentra treatment planning system

Oncentra treatment planning version 3.2.303 (Nucletron B.V., 3900 AX VENENDAAL, The Netherlands), which is shown in Fig. 3.5, is a treatment planning for brachytherapy. It is volume-based planning system that includes state-of-the-art optimization algorithms to ensure efficient treatment planning.

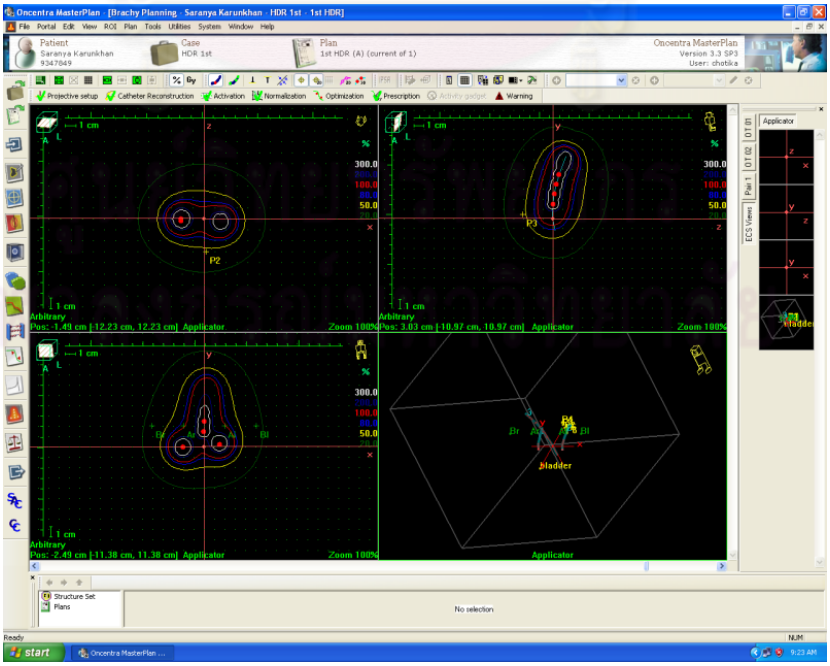

Fig. 3.5, Oncentra treatment planning system.

3.6.3 Head and neck patient image

a. CT simulator scanner

The 4 slice CT scanner (LightSpeed RT GE Medical system, Waukesha, WI, USA.), which is shown in Fig. 3.6, has the ability to simultaneously collecting 4 rows of scan data. The distance from tube to isocenter is 606 mm. The distance from tube to detector focus is 1062 mm. Bore diameter is 800 mm which allows images to be reconstructed with a larger field of view than a standard CT system. Additional software for treatment planning is virtual simulation software which can reconstructed raw image into 3D image and can generate DRR (digital reconstructed radiograph) in many directions. Furthermore, this software allow radiation oncologist to plan treatment and mark point on patient via moving laser in CT room directly.

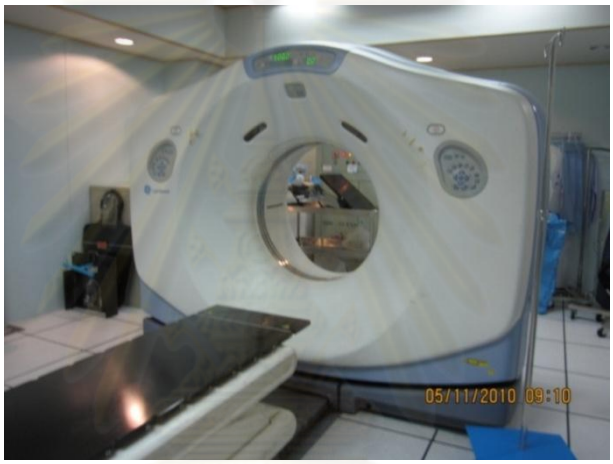

Fig. 3.6, GE planning CT.

b. Varian conebeam CT

Varian cone-beam CT (Version 2.1.2) is a three dimensional imaging modality that become available on linear accelerators. It mounted at 90^{o} on the gantry of linear accelerator. The imager support arm carries an amorphous silicon detector with an active rectangular imaging area of 397 X 298 mm. For the bow-tie filter is a mechanical device that is mounted in front of the tube to filter the X-ray beam. Made of Aluminum for OBI, this device is used to improve the quality of the CBCT projections, which are reconstructed into 3D CBCT images. There are two bow-tie filters provided; a full-fan bow-tie, which is used for acquisition of head scans and the half-fan bow-tie, which is used for acquisition of body scans. The advantages of bow-tie are:

- Reduced skin doses.
- Reduced X-ray scatter, which results in improved image quality.
- Reduced charge trapping in the detector.
- Allow large X-ray techniques to be used without saturating the detector.

For the rotation, the gantry must rotate through slightly more than 360^{o} for a full scan and 200^{o} for a half scan.

CBCT is a high-resolution, low-dose digital imaging system that allows users to confidently manage patient and target movement – both before and during treatments, with 3 modes of kilovoltage (kV) imaging: digital radiographic, cone-beam CT (CBCT), and fluoroscopic imaging. The image and its information which acquired from CBCT on offline review software on on-board imager (OBI) workstation can be imported to TPS in treatment planning room to analyze the image registration uncertainty in head and neck patient in this study.

The linear accelerator equipped with CBCT is shown in Fig. 3.7.

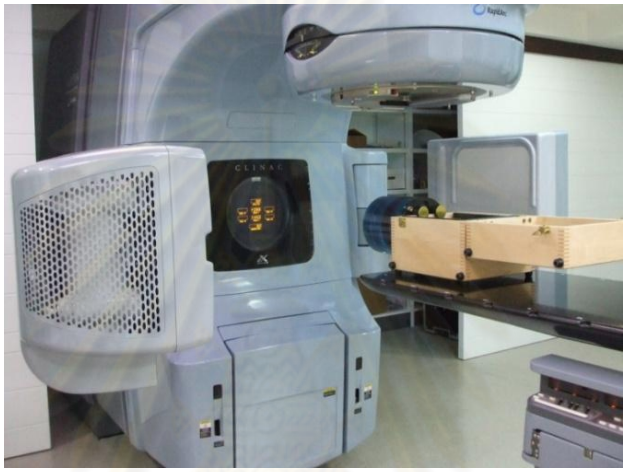

Fig. 3.7, Varian linear accelerator with CBCT.

3.6.4 Manufacturer cylindrical QA phantom

QA Phantoms for imaging machines are accurate complex products. Designed to simulate the human body, they contain several types of strata, in this case air water and PMMA, which are accurately combined to deliver the sharp outlines and contrasts needed to calibrate a mixed X-Ray and CT scanner. This phantom is shown in Fig. 3.8.

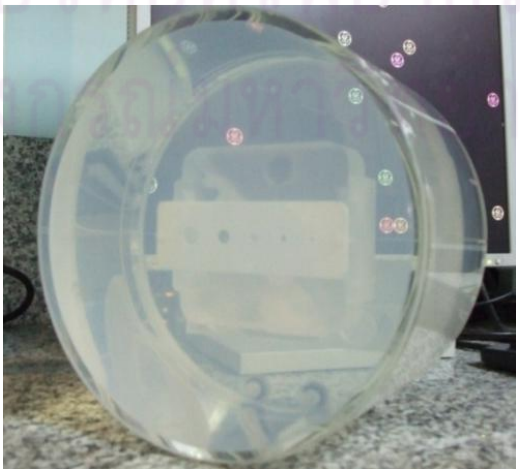

Fig. 3.8, Manufacturer cylindrical QA phantom.

3.6.5 Catphan phantom

The phantoms are used to complete comprehensive performance evaluations of axial, spiral and multi-slice CT scanners and to implement quality assurance programs. The Catphan phantoms are constructed from modules that fit snugly into a durable 7.9"(20 cm) housing. The modules used in the Catphan 504 are made from solid-cast materials. This construction eliminates material absorption of water and leaks associated with water bath phantoms, as well as problems related to varied water sources.

The test modules included with Catphan phantoms are used to conduct a variety of test measurements, including evaluations of the following:

- Scan slice geometry (slice width and slice sensitivity profile)
- High resolution (up to 20 or 21 line pairs per cm)
- Phantom position verification
- Patient alignment system check
- Low contrast sensitivity
- Comparative sub-slice and supra-slice low contrast sensitivity
- Spatial uniformity
- Scan incrementation
- Noise (precision) of CT systems
- Circular symmetry
- Sensitometry (linearity)
- Pixel (matrix) size
- Point spread function and modulation transfer function (MTF) for the x, y, and z axes.

The Catphan phantom is shown in Fig. 3.9.

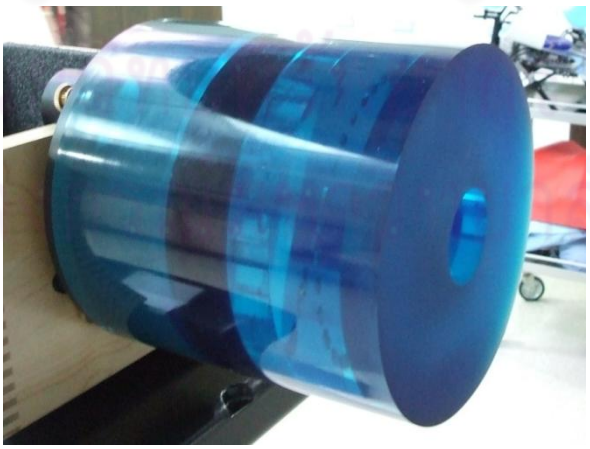

Fig. 3.9, Catphan phantom 504.

3.7 Methods

As an essential prerequisite for the treatment planning process and, in particular for the correlation process, the image that were converted into the treatment planning system must reflect the real geometry of the patient, possible distortions of the images had to be minimized. In addition, the accuracy of the registration software in the treatment planning program was essential. So this study would start with the quality assurance of data transferred to treatment planning systems (Eclipse and Oncentra) included the method of automatic registration in each treatment planning system.

3.7.1 QA of data transferred to treatment planning systems (TPS)

3.7.1.1 Image input using the manufacturer cylindrical QA phantom for CT scanning

The cylindrical QA phantom was scanned with the GE LightSpeed CT. Parameters for scanning were 120 kVp, smart mA (automatic exposure control mode: AEC), matrix 512 X 512. The image datasets of phantom had different slice thickness of 1.25, 2.5, 3.75, 5 and 10 mm, large and small FOV. The QA of data transferred from CT to treatment planning system were performed as the followings:

a. Scan parameter consistency

Different field of view within one CT data set might give wrong dimensions of the phantom or patient. A CT image dataset for 10 mm slice thickness of two different field of views, large and small, were introduced into Eclipse and Oncentra TPSs. The TPS should show no warning. The dimensions of the phantom were measured with the ruler tool from the TPS.

b. Slice thickness

A set of CT scanned with varying slice thickness of 1.25, 2.5, 3.75 and 5 mm, was transferred to both TPSs. The system should not give any warning or comment. This illustrated that the construction of the volume was performed correctly.

c. CT number representation

The homogeneous slice of image dataset was transferred to both TPSs to observe CT number by determining mean and standard deviation of CT number in a region of interest (ROI) 2 X 2 cm^2 size, it is shown in Fig. 3.10. The CT number was compared with the original CT numbers measured on CT workstation.

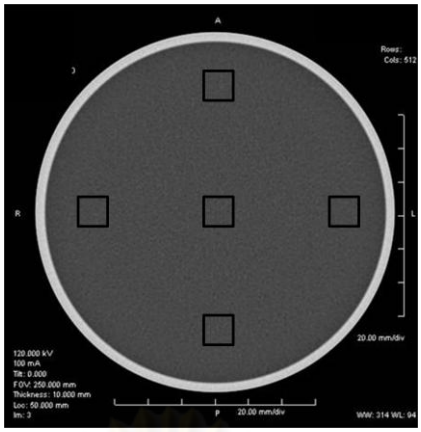

Fig. 3.10, Placing of ROI for CT number measurement.

d. Images geometry reconstruction

CT image datasets of line pair part of QA phantom were imported to both TPSs. The distance between the gap and the angle of ramp which shown in Fig. 3.11 were measured in TPS and on the phantom. These values were compared between those measured from TPS and phantom.

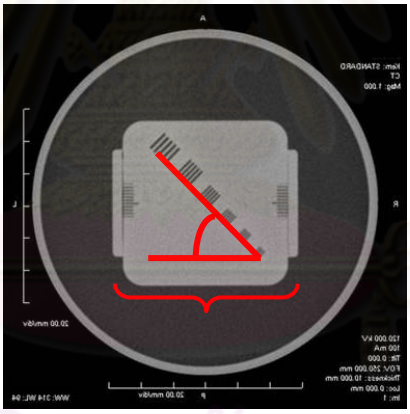

Fig. 3.11, Measurement of position on QA phantom image dataset.

3.7.1.2 Image input using the Catphan phantom for conebeam CT scanning

The Catphan phantom was scanned by Varian CBCT with standard – dose head mode which operated at 100 kVp, 145 mAs, 360 projections and 384 X 384 matrix. The reconstructed slice thickness was 2.5 mm. The process of QA of data transferred was performed by the following.

a. CT number representation

CBCT image dataset of contrast sensitometric part of Catphan phantom was imported to Eclipse TPS. The CT number in the TPS was determined in term of the mean and standard deviation in a region of interest (ROI) 7 X 7 mm^2 size, it is shown in Fig. 3.12, the reading values were compared with the standard CT number of each material. The materials were acrylic, derlin, air, Teflon, PMP, LDPE and polystyrene.

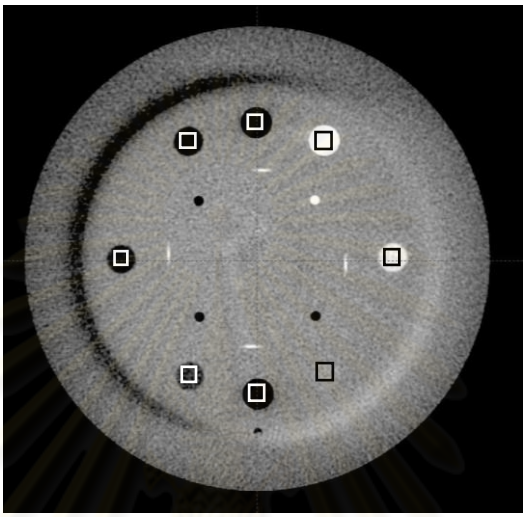

Fig. 3.12, Measurement of CT number on CBCT image dataset.

b. Image geometry reconstruction

CBCT image dataset of uniform module Catphan phantom was imported to Eclipse TPS. The size of Catphan phantom image along X and Y axes were measured by ruler tool of TPS. These values were compared with the real size of phantom.

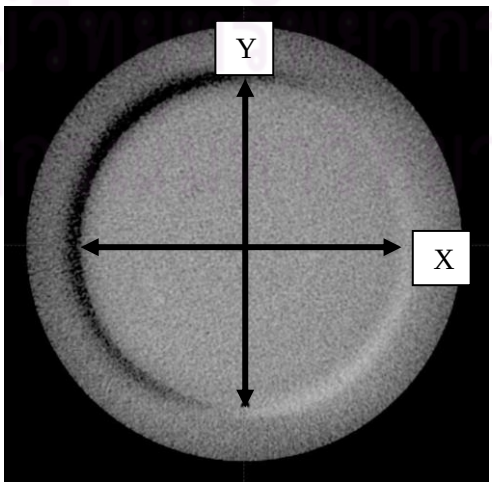

Fig. 3.13, Measurement of CBCT image dataset of Catphan phantom.

3.7.1.3 Image input using density phantom generated from ImSim QA software

Image dataset that was used in this part was simulated phantom which generated from ImSim QA software. ImSim QA software had three types of phantom there were density phantom for QA of ImSim, Simple brain phantom for registration by mutual information method and branch phantom for registration by match point method. These three types of phantom are shown in Fig. 3.14.

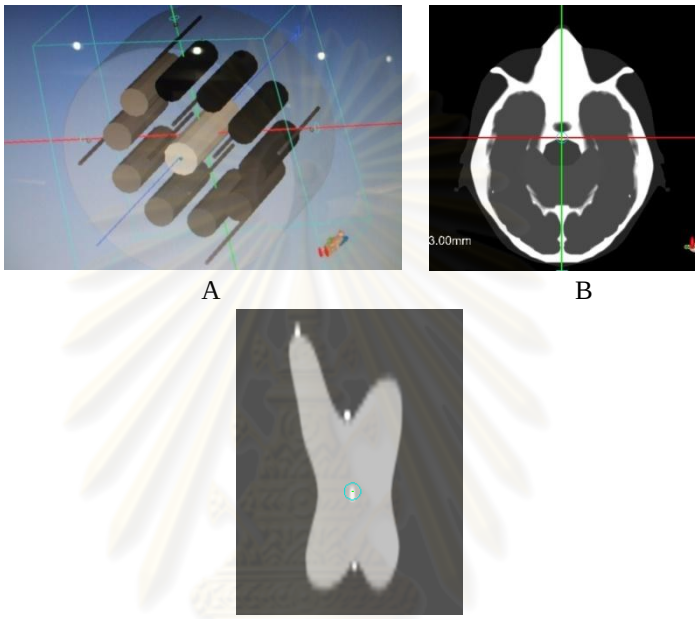

Fig. 3.14, A) Density phantom, B) Simple brain phantom and C) Branch phantom

a. CT number representation

CT number was generated on homogeneous phantom using ImSim QA software. CT data of generated phantom was imported in both TPSs and the CT number in a ROI was determined as shown in Fig. 3.15. These values were compared with the original number generated from ImSim.

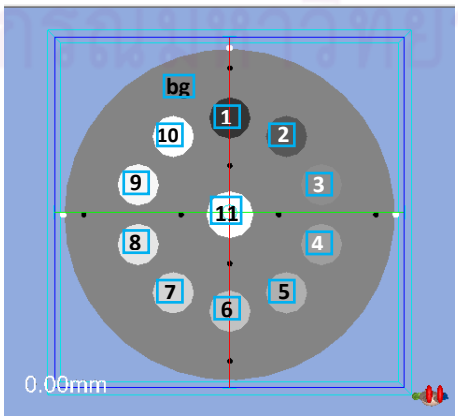

Fig. 3.15, Measurement position of CT number on density phantom.

b. Image geometry

The image dataset of whole generated phantom from ImSim was imported in both TPSs. The size of inner cylindrical in X, Y, and Z axes were measured in TPS which shown in Fig. 3.16. This result was compared with ImSim data.

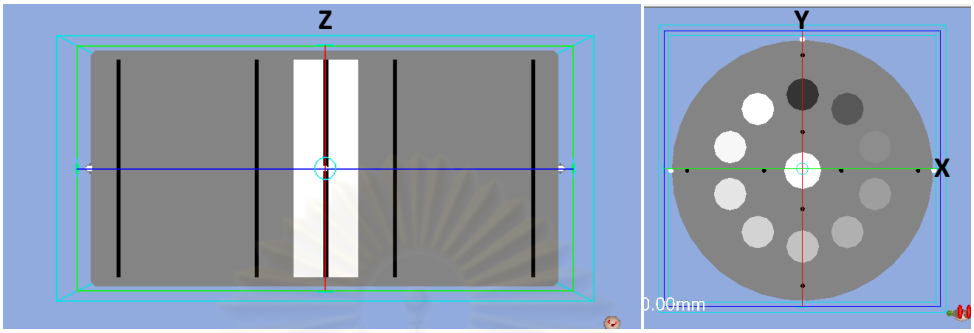

Fig. 3.16, Measurement along X, Y and Z axes in density phantom.

3.7.2 Verification of image registration methods in TPS using ImSim QA software

The methods that verified were mutual information method and match point method. The verification method was performed by the following.

3.7.2.1 ImSim images transformation

There were stationary image dataset, translation image dataset by translating on each axis of X, Y and Z at 5, 10 and 15 mm. and the translation in all axes simultaneously at 5, 10 and 15 mm. The last one was rotation image dataset, the rotating of 5, 10 and 15 degree were performed in each axis and also all axes in the same manner as the translation. The dataset of transformed images are shown in Table 3.1 which included 25 sets.

Table 3.1, The image dataset generated from ImSim QA software.

Stationary set	No transformed	(0, 0, 0)
Translation set	5, 10, 15 mm	(5, 0, 0), (0, 5, 0), (0, 0, 5), (10, 0, 0), (0, 10, 0), (0, 0, 10), (15, 0, 0), (0, 15, 0), (0, 0, 15), (5, 5, 5), (10, 10, 10), (15, 15, 15)
Rotation set	5, 10, 15 degree	(5, 0, 0), (0, 5, 0), (0, 0, 5), (10, 0, 0), (0, 10, 0), (0, 0, 10), (15, 0, 0), (0, 15, 0), (0, 0, 15), (5, 5, 5), (10, 10, 10), (15, 15, 15)

3.7.2.2 Mutual information method

Simple brain phantom which had three image datasets as described above generating by ImSim QA software was registered on Eclipse TPS and Oncentra TPS.

3.7.2.3 Match point method

Branch phantom which had specific point generating by ImSim QA software and had three sets were registered on Eclipse TPS and Oncentra TPS. In this method the 6 specific points were selected to mark for match point processing.

3.7.3 Verification of image registration methods of TPS using head and neck patient image

After phantom image dataset was employed to verify mutual information and match point method of registration, the head and neck patient image was selected to verify the two methods of image registrations for clinical application in patient setup verification. All patients were delivered CBCT imaging to verify the position in treatment room at the first day of treatment program. The method was performed by the following:

3.7.3.1 Data acquisition

Image acquisition for treatment planning was performed by computing tomography (CT) and conebeam CT. They were used for patient setup verification before receiving the treatment. These complementary aspects could be integrated into treatment planning by correlation of the images from different modalities.

The planning CT imaging parameters were 120 kVp, smart mA (automatic exposure control mode: AEC), matrix 512 X 512. The reconstructed slice thickness was 2.5 mm. During the scan, patients were immobilized in the supine position with a thermoplastic mask.

CBCT image dataset was acquired under standard- dose head mode which had 100 kVp, 145 mAs, 360 projections and 384 X 384 matrix. The reconstructed slice thickness was 2.5 mm. During the scan, patients were immobilized in the supine position with a thermoplastic mask and were positioned the same as performing CT imaging.

The examples of head and neck patient image datasets from planning CT and CBCT modalities are shown in Fig. 3.17.

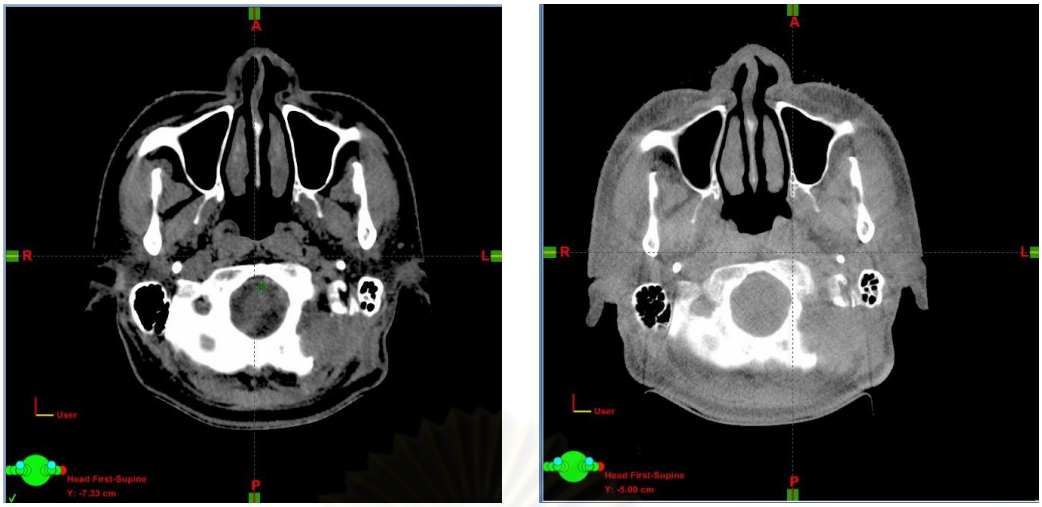

A B

Fig. 3.17, A) Planning CT image dataset and B) CBCT image dataset of head and neck patient.

3.7.3.2 Head and neck patient image dataset

Planning CT image dataset of 20 head and neck patients were selected as the stationary image dataset (reference image) and the corresponded CBCT image dataset of 20 patients on the first day treatment were selected to be the moving image dataset.

3.7.3.3 Imported data

These two image datasets were imported to Eclipse TPS.

3.7.3.4 Registration

CBCT image dataset was registered with planning CT image dataset by mutual information and match point method. For match point method, the 4 selected points were marked on specific anatomy of head and neck by observers who expert in anatomical structure.

3.8 Outcome measurement

Variable: independent variables	=	image registration method, TPS
: dependent variables	=	registration error, registration deviation

3.9 Data collection

The measurement of registration error and registration deviation was collected in distance (mm, cm) and rotated (degree) for Eclipse and Oncentra TPSs.

3.10 Data analysis

3.10.1 Phantom image dataset registration by ImSim QA software

For Eclipse TPS, the position shift by mutual information and match point methods were reported by registration property that included in the software. These shift values were compared with the actual shifts that were applied by ImSim QA software. The registration error was occurred when these two values were different.

For Oncentra TPS, the distant measurement of the same point on reference and moving image dataset of phantom was performed by an observer. The difference in measurement was registration error for these two registration methods.

3.10.2 Head and neck patient image dataset registration

This image dataset of CBCT could be imported from OBI workstation only to Eclipse TPS to registered with planning CT. So, the position shift value was determined by Eclipse TPS method. The coordinate of optimized image registration by radiation oncologist on the OBI workstation on the first day was used as the gold standard. The registered coordinates by the two methods of auto image registration between planning CT and CBCT were determined and the differences in the coordinate between optimized by radiation oncologist and auto method were the deviation of image registration method.

3.11 Benefit of the study

- Assist the radiation oncologist to optimize the position shift easily and reliably by suitable image registration method.
- Improve planning target volume (PTV) delineation.
- Accurate dose to target volume and organ at risk.

3.12 Ethical consideration

Although this study was performed in phantom and used image of patient, however the ethical approval was processed by Ethics Committee of Faculty of medicine, Chulalongkorn University.

CHAPTER IV

RESULTS

4.1 QA of data transferred to treatment planning systems (TPS)

4.1.1 Image input using the manufacturer cylindrical QA phantom for CT scanning

The signal loss during the data transformation from CT workstation to Eclipse and Oncentra TPSs considered CT number reading at various position of phantom was within tolerance values of 20 and image reconstruction had the accurate dimension within 2 mm [19] for all image datasets of different slice thickness and fields of view studied. The result was shown as follows:

a. Scan parameter consistency

Both TPSs has given no warning when imported CT image dataset with slices of two difference field of view, large and small for 10 mm slice thickness. The dimensions of the phantom were measured with the ruler tool from each TPS and the results shown in Fig. 4.1 and 4.2 illustrated the same value for large and small FOV in both TPSs.

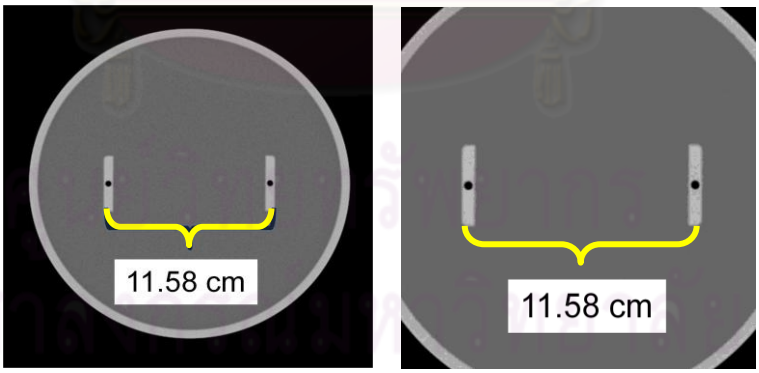

A B

Fig. 4.1, Measurement of A) large and B) small FOV of CT image dataset with the ruler tool from Eclipse TPS.

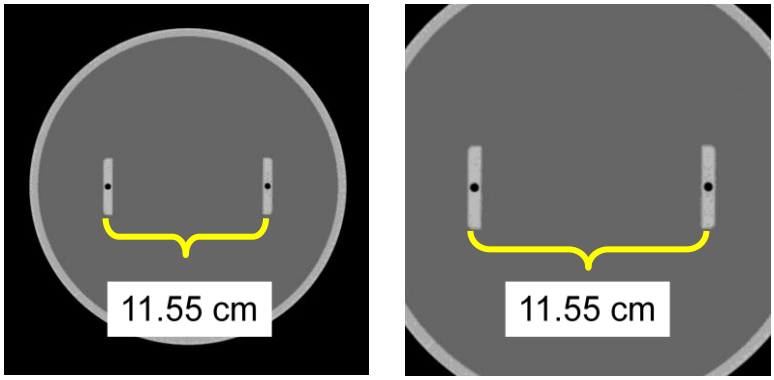

A B

Fig. 4.2, Measurement of A) large and B) small FOV of CT image dataset with the ruler tool from Oncentra TPS.

b. Slice thickness

When importing of CT image dataset with varying slice thickness, both TPSs did not give any warning or comment. This means that the construction of the volume was performed correctly.

c. CT number representation

The result of CT number consistency in water which was a part of phantom is shown in Table 4.1 and 4.2. The error range of CT number measured by Eclipse TPS was 0.03 – 0.33 and measured by Oncentra TPS was 0.04 – 1.19.

Table 4.1, CT number error reading from Eclipse TPS and CT workstation.

	CT No.				
	upper	**lower**	**center**	**right**	**left**
CT Workstation	0.90±2.41	0.36±2.69	1.03±2.69	0.85±2.49	0.57±2.58
Eclipse TPS	1.20±2.25	0.30±2.75	1.00±2.47	1.00±2.47	0.90±2.65
Error	0.30	0.06	0.03	0.25	0.33

Table 4.2, CT number error reading from Oncentra TPS and CT workstation.

	CT No.				
	upper	**lower**	**center**	**right**	**left**
CT Workstation	0.90±2.41	0.36±2.69	1.03±2.69	0.85±2.49	0.57±2.58
Oncentra TPS	0.86±2.59	0.06±2.74	2.22±2.75	0.17±2.8	1.67±2.96
Error	0.04	0.30	1.19	0.68	1.10

d. Images geometry reconstruction

The geometry measurement by both TPSs compared with phantom measurement is shown in Table 4.3 and 4.4. The errors of measurement of Eclipse TPS were 0.14 mm and 0.1 degree and error of Oncentra TPS measurement were 0.17 mm and 0.45 degree.

Table 4.3, Measurement comparison between phantom and image data on Eclipse TPS.

	Distance between gap	Slope of ramp
Phantom	11.3 mm	44.9 degree
Eclipse	11.44 mm	45 degree
Error	0.14 mm	0.1 degree

Table 4.4, Measurement comparison between phantom and image data on Oncentra TPS.

	Distance between gap	Slope of ramp
Phantom	11.3 mm	44.9 degree
Oncentra	11.47 mm	45.35 degree
Error	0.17 mm	0.45 degree

4.1.2 Image input using the Catphan phantom for conebeam CT scanning

a. CT number representation

The result of CT number measurement from Eclipse TPS is shown in Table 4.5, the measurement was compared with the standard CT number for each material. The error range of CT number measurement was 0.2 – 19.

Table 4.5, CT number error reading from Eclipse TPS compared with standard CT number of material.

	Air (-1000)		**Acrylic**	**Derlin**	**Teflon**	**PMP**	**LDPE**	**Polystyrene**
	upper	**lower**	**(120)**	**(340)**	**(990)**	**(-200)**	**(-100)**	**(-35)**
Measure CT	-997.7 ±4.96	-994.9 ±11.91	124.3 ±34.80	359.0 ±29.36	1008.2 ±30.64	-201.7 ±24.91	-99.8 ±31.06	-37.3 ± 31
Error	2.3	5.1	4.3	19	18.2	1.7	0.2	2.3

b. Images geometry reconstruction

The measurement of the size of phantom in Eclipse TPS compared with the real size of phantom is shown in Table 4.6.

Table 4.6, Compare measurement between phantom and image data on Eclipse TPS.

	X axis (cm)	**Y axis (cm)**
Real phantom	15	15
Measurement in Eclipse	15.14	14.92
Error	0.14	0.08

4.1.3 Image input using density phantom generated from ImSim QA software

For ImSim QA software, the value of CT number in each region which shown in Fig. 3.13 and size of phantom along X, Y and Z axes were comparable with the value that displayed in Eclipse and Oncentra TPSs. The result of quality assurance of ImSim QA software was illustrated as follows:

a. CT number representation

The result of CT number displayed in each TPS was shown in Table 4.7 and 4.8. The error range in Eclipse TPS was 1 – 9 and in Oncentra TPS was 0 – 8.

Table 4.7, CT number error reading from Eclipse TPS and ImSim QA software.

	CT No.											
	1	2	3	4	5	6	7	8	9	10	11	bg
ImSim	-400	-200	100	200	300	400	500	600	700	800	1000	20
Eclipse TPS	-409	-205	95	191	299	395	491	599	695	791	995	11
Error	9	5	5	9	1	5	9	1	5	9	5	9

Table 4.8, CT number error reading from Oncentra TPS and ImSim QA software.

	CT No.											
	1	2	3	4	5	6	7	8	9	10	11	bg
ImSim	-400	-200	100	200	300	400	500	600	700	800	1000	20
Oncentra TPS	-408	-204	96	192	300	396	492	600	696	792	996	28
Error	8	4	4	8	0	4	8	0	4	8	4	8

b. Image geometry

The measurement of density phantom by both TPSs was compared with value generated from ImSim QA software. The results are shown in Table 4.9 and 4.10, the error range measured from Eclipse TPS was 0.38 – 0.42 mm and error range from Oncentra TPS was 0.89 – 1.88 mm.

Table 4.9, Geometry measurement of density phantom along X, Y and Z axes by Eclipse TPS.

	X (mm)	**Y (mm)**	**Z (mm)**
ImSim	38.71	38.71	117.42
Eclipse TPS	38.33	39.10	117.00
error	0.38	0.39	0.42

Table 4.10, Geometry measurement of density phantom along X, Y and Z axes by Oncentra TPS.

	X (mm)	**Y (mm)**	**Z (mm)**
ImSim	38.71	38.71	117.42
Oncentra TPS	39.70	39.60	119.30
error	0.99	0.89	1.88

4.2 Registration of ImSim phantom image dataset

Using phantom that was generated from ImSim QA software for stationary, translation and rotation image datasets, the registration errors from mutual information and match point registration methods in Eclipse TPS were within 0.34 mm when registered with translation set. For rotation set, registration error was within 0.95 mm. The registration errors are shown in Table 4.11 and 4.12. From these results, the average registration error was less at the z direction, it was greatest when applying transformation in all axes simultaneously which is shown in Fig. 4.3 and 4.4.

Table 4.11, Registration error from registered by mutual information method in Eclipse TPS.

Applied transformation	X axis (mm)	Y axis (mm)	Z axis (mm)	XYZ axes (mm)	Average (mm)
Translation: 5mm	0.03	0.03	0.02	0.08	0.04
Translation: 10 mm	0.00	0.04	0.02	0.28	0.09
Translation: 15 mm	0.14	0.12	0.11	0.04	0.10
Rotation: 5 degree	0.10	0.02	0.02	0.18	0.08
Rotation: 10 degree	0.18	0.19	0.02	0.34	0.18
Rotation: 15 degree	0.18	0.17	0.05	0.28	0.17
Average (mm)	0.11	0.10	0.04	0.20	0.11

Table 4.12, Registration error from registered by match point method in Eclipse TPS

Applied transformation	X axis (mm)	Y axis (mm)	Z axis (mm)	XYZ axes (mm)	Average (mm)
Translation 5mm	0.14	0.04	0.14	0.23	0.13
Translation 10 mm	0.10	0.18	0.14	0.25	0.17
Translation 15 mm	0.09	0.13	0.31	0.34	0.22
Rotation 5 degree	0.23	0.29	0.05	0.24	0.20
Rotation 10 degree	0.29	0.44	0.12	0.49	0.34
Rotation 15 degree	0.51	0.62	0.06	0.95	0.54
Average (mm)	0.23	0.28	0.14	0.42	0.27

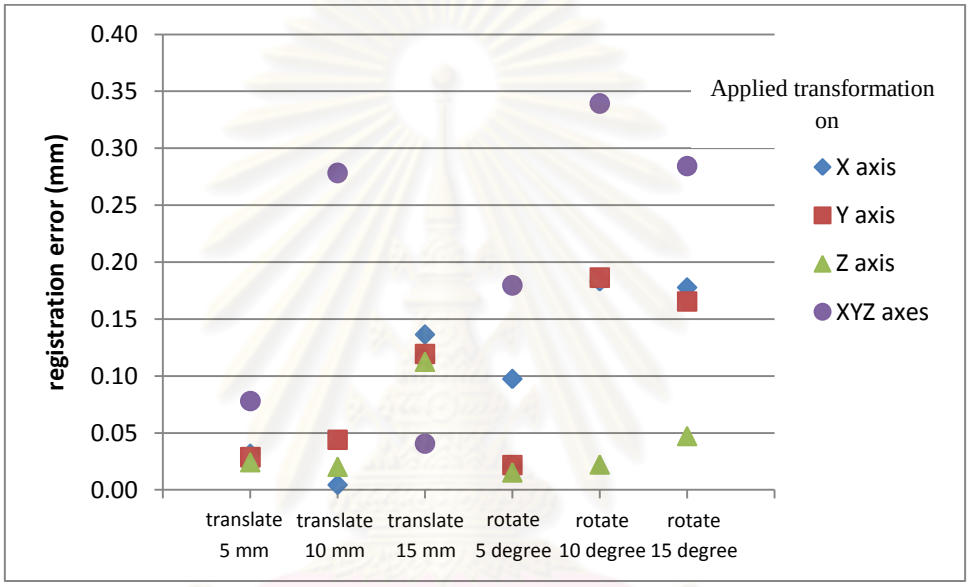

Fig. 4.3, Registration error from mutual information method in Eclipse TPS.

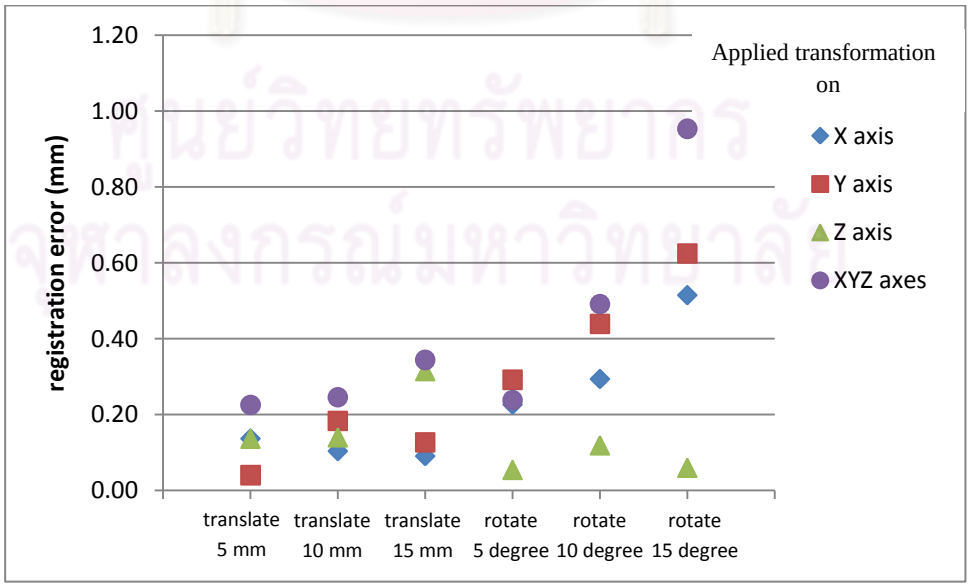

Fig. 4.4, Registration error from match point method in Eclipse TPS.

For Oncentra TPS, the results from these two methods of registration are shown in Table 4.13 and 4.14 and in Fig. 4.5 and 4.6. Registration error was less than 0.05 ± 0.02 cm for registration with translation set and for rotation set registering, the registration error was less than 0.33 ± 0.08 cm. The graphs showed higher registration error which was the same as in Eclipse when applying transformation in all axes.

Table 4.13, Registration error from registered by mutual information method in Oncentra TPS.

Applied transformation	X axis (cm)	Y axis (cm)	Z axis (cm)	XYZ axes (cm)	Average (cm)
Translation 5mm	0.02	0.01	0.02	0.03	0.02
Rotation 5 degree	0.07	-	-	-	0.07
Rotation 10 degree	0.13	0.08	0.03	0.17	0.10
Average (cm)	0.07	0.05	0.03	0.10	0.06

Table 4.14, Registration error from registered by match point method in Oncentra TPS.

Applied transformation	X axis (cm)	Y axis (cm)	Z axis (cm)	XYZ axes (cm)	Average (cm)
Translation 5mm	0.00	0.02	0.05	0.04	0.03
Rotation 5 degree	0.05	0.13	0.03	0.15	0.09
Rotation 10 degree	0.10	0.10	0.03	0.33	0.14
Average (cm)	0.05	0.08	0.04	0.17	0.09

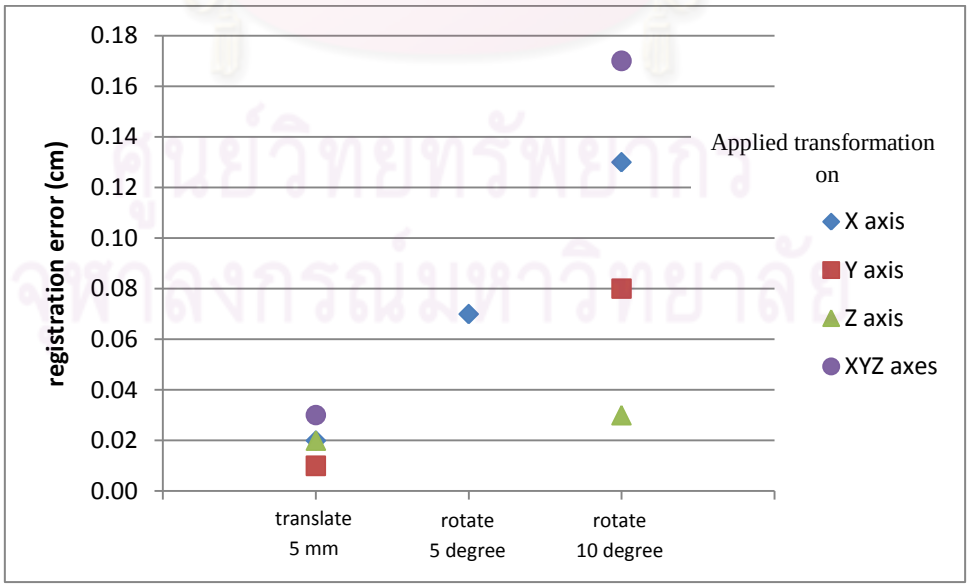

Fig. 4.5, Registration error from mutual information method in Oncentra TPS.

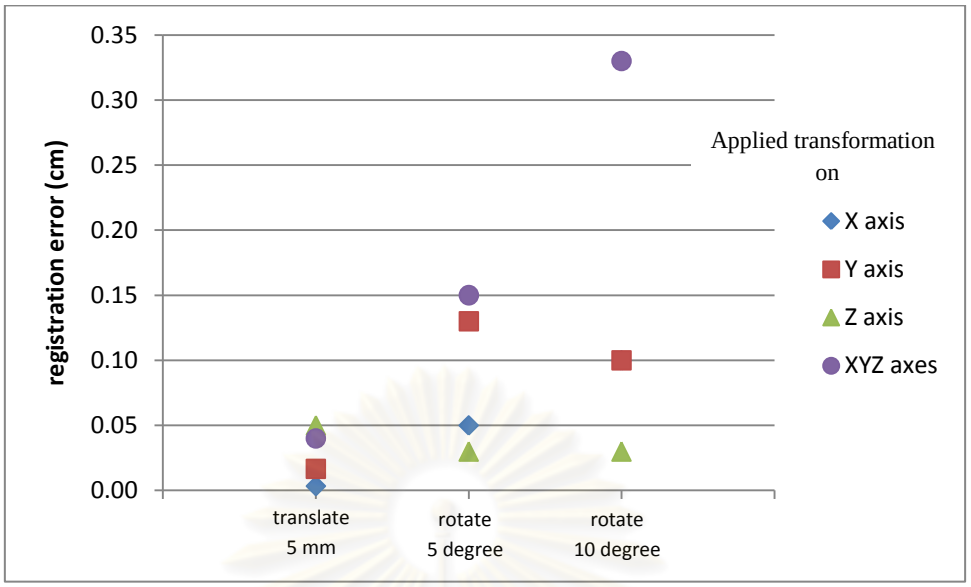

Fig. 4.6, Registration error from match point method in Oncentra TPS.

For the verification of registration methods, the mutual information gave slightly better result than match point method in both TPSs, which shown in Fig. 4.7 and 4.8. The mean registration errors in all axes for both methods were less than 1.5 mm in both TPSs.

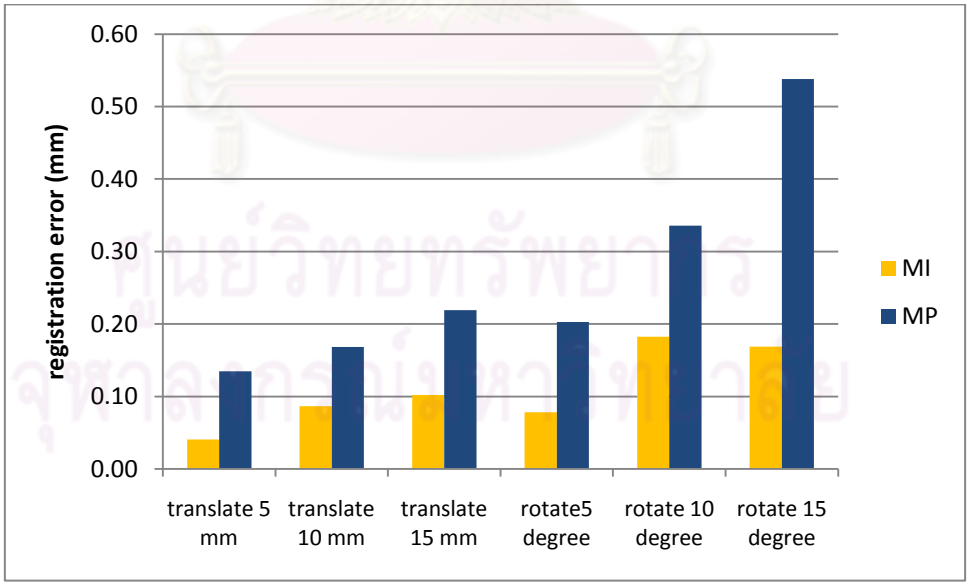

Fig. 4.7, Comparison of registration error between mutual information (MI) and match point (MP) methods in Eclipse TPS.

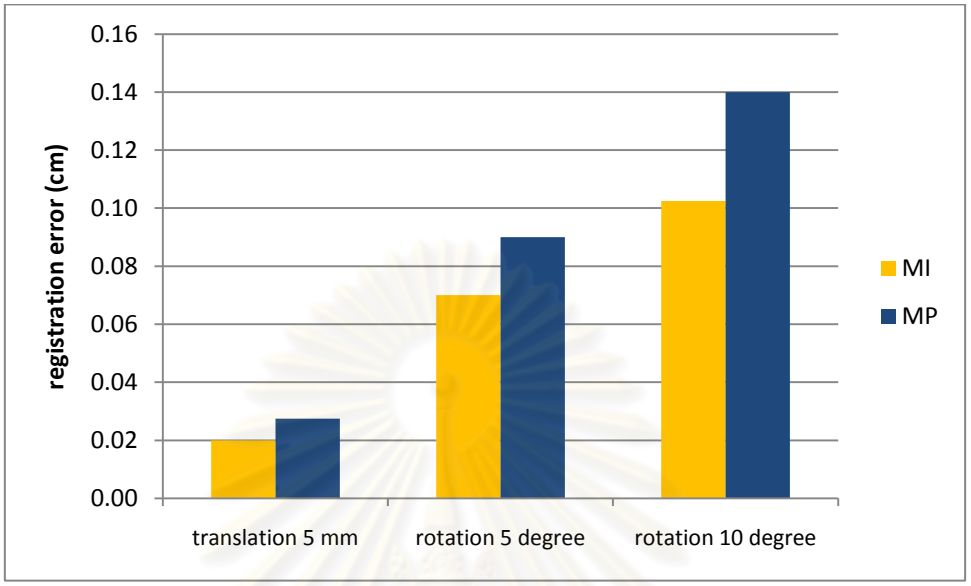

Fig. 4.8, Comparison of registration error between mutual information (MI) and match point (MP) methods in Oncentra TPS.

4.3 Registration of CBCT and planning CT patient image datasets

The deviation of mutual information and match point registration from registered optimization by radiation oncologists are listed in Table 4.15 and 4.16, respectively. For mutual information method, the mean deviation was 2.02 ± 2.00 mm (0 – 8.87 mm) translation and 0.82 ± 1.16 degree (0 – 6.89 degree) rotation. For match point method, the mean deviation was 3.05 ± 2.92 mm (0.02 – 17.86 mm) translation and 1.31 ± 1.35 degree (0 – 6.62 degree) rotation.

Table 4.15, Deviation of mutual information image registration from optimization by radiation oncologist.

Case	Translation (mm)			Rotation (degree)		
	X	Y	Z	X	Y	Z
1	8.87	4.01	2.31	0.12	1.64	2.15
2	4.89	5.47	4.32	0.57	1.73	1.79
3	1.14	0.19	3.53	0.40	0.50	2.49
4	0.81	0.03	1.00	0.39	0.57	1.65
5	0.64	0.51	1.10	0.30	0.31	0.94
6	0.05	3.12	1.14	0.09	0.00	0.97
7	0.60	1.16	0.45	0.29	0.41	1.08
8	3.55	1.33	3.12	0.04	0.06	0.47
9	1.44	0.35	0.00	0.15	0.57	3.28
10	0.14	0.15	2.39	0.04	0.82	0.43
11	0.22	0.22	1.46	0.03	0.01	0.34
12	0.02	1.05	0.57	0.04	0.06	1.17
13	1.79	0.14	1.41	0.06	0.47	0.08
14	0.86	1.21	3.67	0.24	0.20	0.74
15	2.35	1.95	1.81	0.86	0.04	0.13
16	4.86	4.02	2.19	1.02	0.02	1.56
17	1.49	2.90	5.70	0.31	1.99	1.08
18	0.67	1.02	1.45	0.12	0.07	0.27
19	1.24	0.22	1.69	0.32	0.38	0.37
20	5.40	8.65	2.92	6.89	1.63	4.26

Table 4.16, Deviation of match point image registration from optimization by radiation oncologist.

Case	Translation (mm)			Rotation (degree)		
	X	Y	Z	X	Y	Z
1	9.68	5.52	3.10	0.78	1.67	2.39
2	4.46	4.33	5.57	1.18	3.99	1.15
3	1.57	0.80	3.76	0.22	0.30	2.70
4	1.23	0.24	1.52	0.39	0.97	1.54
5	6.52	3.19	0.99	0.18	0.05	1.93
6	3.13	3.43	2.28	3.38	0.14	0.80
7	1.80	2.38	1.32	0.31	0.00	0.95
8	2.64	1.49	4.02	1.71	1.44	0.25
9	0.94	1.40	0.10	1.95	2.03	0.86
10	1.62	1.59	2.13	0.93	0.25	0.08
11	0.88	0.63	0.80	0.04	0.10	0.03
12	0.19	0.85	0.02	3.36	1.50	0.56
13	1.04	0.18	3.76	1.24	0.00	0.05
14	1.05	3.83	2.54	0.39	0.48	1.58
15	3.70	0.95	4.42	1.96	0.62	0.74
16	6.39	3.96	17.86	5.60	0.31	2.13
17	2.12	3.36	8.85	1.85	1.67	1.32
18	2.03	0.91	1.73	0.59	0.23	0.55
19	3.11	2.60	4.51	3.87	2.19	0.42
20	5.66	8.59	3.86	6.62	1.97	1.99

For these two registration methods, the mutual information method gave the less registration deviation in clinical used compared with match point method. The deviation of translation and rotation of these two methods are shown and compared in Fig. 4.9 and 4.10.

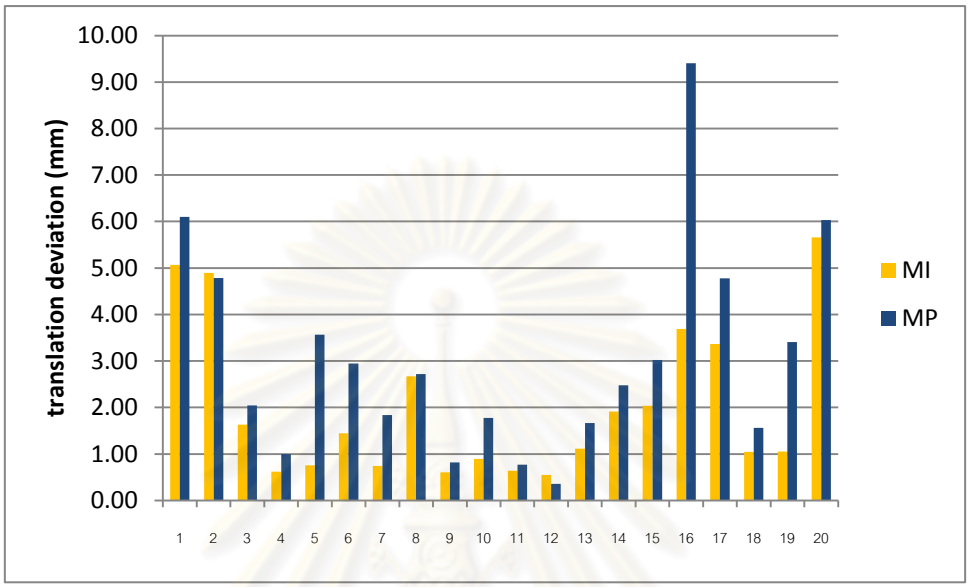

Fig. 4.9, Translation deviation of mutual information (MI) and match point (MP) methods in head and neck patient image.

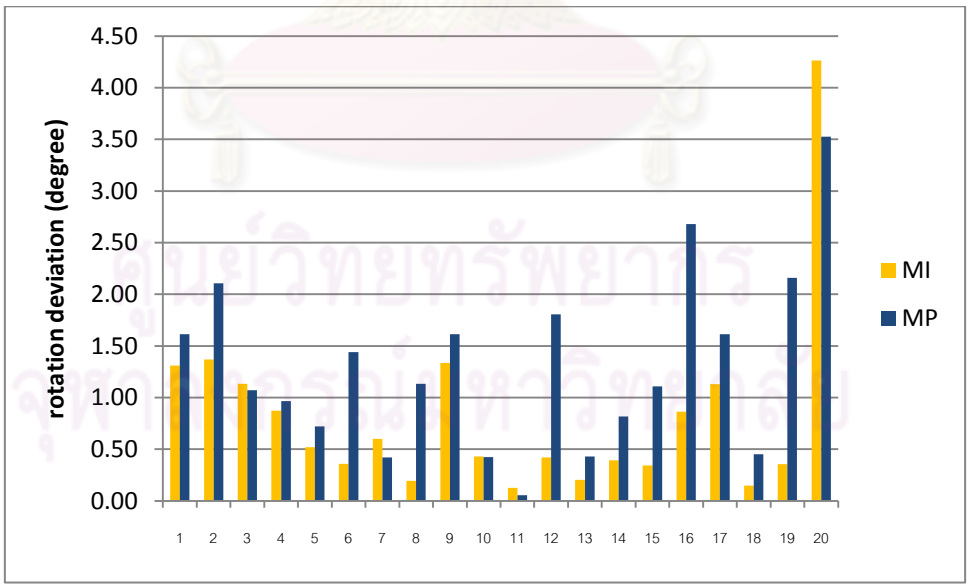

Fig. 4.10, Rotation deviation of mutual information (MI) and match point (MP) methods in head and neck patient image.

CHAPTER V

DISCUSSION AND CONCLUSION

5.1 Discussion

The image registration accuracies arising from IGRT process are (a) the accuracy of the spatial coordinates of the image with respect to the megavoltage (MV) treatment beam, (b) the accuracy in image registration and (c) the accuracy of patient re-positioned [14]. The accuracy of the spatial coordinate of the image can be minimized from the QA of the TPS and the megavoltage machine. The uncertainty which called registration error can be determined by many methods [1, 16, 17, 18]. If the factors (a) and (b) are eliminated, the accuracy of patient position could be acquired. The introduction of ImSim software (Modus Medical Devices Inc., North Routledge Park London, Canada) can solve the parameter influence such as, coordinate accuracy and movement of the marker, so the actual image registration error caused by software of registration could be determined.

The registration errors using ImSim software for Eclipse and Oncentra TPSs are slightly different. The maximum registration errors from Eclipse and Oncentra TPS with the simultaneous translation and rotation in all axes are shown in Table 5.1. Eclipse TPS gives slightly better result than Oncentra TPS in both translation set and rotation set of registration.

The registration error from Eclipse and Oncentra TPS increases when the degree of transformation is higher. Note that the registration between reference set and apply rotation set contributes the registration error more than registration with apply translation set. The registration with moving set which apply transformation in all axes (X, Y and Z) contributes the registration error more than moving set which apply only one axis, the result agree with the other study [17]. The registration error for the transformation on Z axis of moving set is less than registration error applying transformation in other axes, this may be due to the limitation of ImSim QA software which can display only X and Y plane not Z plane.

Table 5.1, Comparison of maximum registration error from Eclipse and Oncentra TPSs

	Maximum registration error	
	Translation set (mm)	Rotation set (mm)
Eclipse TPS	0.34	0.95
Oncentra TPS	0.50	3.30

For mutual information and match point method, the registration error in graph of Fig. 4.7, 4.8 and Table 5.2 show the better result of mutual information than match point method in all cases of simulated ImSim phantom for both TPSs. The mutual information delivers the better result (less registration error) than match point method because match point method is highly user dependent and relies on the skill of the

user to locate the same point in each image. To minimize the residual registration error, the several iterations is required. So this is not possible in clinical use to perform several times per case to increase accuracy. For mutual information, it uses averaging intensity to match two sets of image. Regardless of the skill of the user in aligning the land mark, mutual information consistently results in more accurate registration [15].

Table 5.2, Comparison of average registration error from mutual information and match point methods.

	Mutual information (mm)	Match point (mm)
Eclipse TPS	0.11	0.27
Oncentra TPS	0.60	0.90

Our work show better result when comparing the average registration error with other studies [1, 15, 16, 17], it is shown in Table 5.3. The other studies used the marker or phantom to determine the registration error which may add the uncertainties, while our method considers only uncertainty from the algorithm.

Table 5.3, The average registration error from mutual information and match point methods compare with other studies.

	Mutual information (mm)	**Match point (mm)**
This study	0.11	0.27
Wang X. et al	1.03	1.03
Plaquin N. and Rangel A.	1	1
Buhl SK. et al.	3	-
Fox T. et al.	0.75	-

The image dataset that is generated by ImSim QA software both reference and moving image dataset have the same characteristic of data such as pixel size, resolution or even contrast of image. The another benefit of this phantom is the setup position, because it has no influence factors such as positioning error from patient setup, anatomy change in patient or even spatial information obtained with different imaging modality. So from this result, the ImSim QA software can reduce uncertainties. Then the registration error arising from the algorithm can be determined. This should be emphasized because all the parameters are deleted.

In head and neck CBCT image registered with planning CT image, we use registering optimization by radiation oncologist in OBI workstation on clinical basis as a gold standard. The mean registration deviation is 2.02 ± 2.00 mm. The deviations occur when comparing coordinate between optimize by radiation oncologist and two methods of auto registration, the maximum difference are more than tolerance value or 2 mm and 2 degree because they include the registration error which occur by the software of registration in TPS, and also the difference of voxel size between planning CT and cone beam CT. Another cause is the optimization from radiation oncologists, sometimes they localize on the interest region not covering the whole

image. However, our results are comparable to other studies. Hou J and Guerrero M [20] reported the mean shift of 2.8 ± 0.2 mm in soft tissue target in evaluation of nine target points in head and neck cancer. The clinical result also illustrated the same way as the ImSim phantom registration that the mutual information gives slightly better result than match point method. This could be explained by the misalignment of reference points in both stationary and moving images.

5.2 Conclusion

The Eclipse TPS contributes slightly better result of registration than Oncentra TPS. The Eclipse TPS is suitable for clinical application to register between planning CT and CBCT for patient setup verification.

From mutual information and match point method of automatic registration, the best one is mutual information method. However, these two methods can provided accurate CBCT and planning CT image registration.

The factors that may influence the image registration process include the dose, FBCT slice width, CBCT and FBCT matrix size, choice of algorithm and selection of the image region to be registered. The further study of these parameter effects should be undertaken in the near future so that the reliable and accurate image registration in image guided radiotherapy could be obtained.

Reference

[1] Ploquin, N., and Rangel, A. Phantom evaluation of a commercially available three modality image guided radiation therapy system. Medical Physics. 35(2008): 5303 – 5311.

[2] Kessler, M. L., and Roberson, M. Image registration and data fusion for radiotherapy treatment planning. The British Journal of Radiology. 79 (2006): S99–S10.

[3] Ping, X., and Quynh – Thu, Le. Image – guided and adaptive radiation therapy. Philadelphia, USA, (2010).

[4] Wikipedia the Free Encyclopedia [online]. Available from http://en.wikipedia.org/wiki/Image-guided_radiation_therapy. {2010, Dec 25}.

[5] Martin, J. M., et al. The management of imaging dose during image-guided radiotherapy: Report of the AAPM Task Group 75. Medical Physics. 34 (2007): 4041 – 4063.

[6] Odero, D.O., and Shimm, D.S. Third party EPID with IGRT capability retrofitted onto an existing medical linear accelerator. Biomedical Imaging and Intervention Journal. Vol. 3: No. 5, (2009).

[7] Wikipedia the Free Encyclopedia [online]. Available from http://en.wikipedia.org/wiki/Fluoroscopy. {2011, Feb 23}.

[8] Jacobson, J.A. Ultrasonography. Available from http://www.merckmanuals.com/professional/sec22/ch329/ch329g.html. {2008, Jul}.

[9] Yartsev, S., Kron, T., and Dyk, J.V. Tomotherapy as a tool in image-guided radiation therapy (IGRT): theoretical and technological aspects. Biomedical Imaging and Intervention Journal. Vol. 1: No. 3, (2007).

[10] Miracle, A.C., and Mukherjia, S.K. Conebeam CT of the head and neck, part: Physical principles. American Journal of Neuroradiology. Available from http://www.ajnr.org/cgi/content/full/30/6/1088. {2009, May 13}.

[11] Wikipedia the Free Encyclopedia [online]. Available from http://en.wikipedia.org/wiki/Image_registration. {2010, Dec 29}.

[12] Bankman, N. I. Handbook of medical image processing and analysis. Elsevier Inc, California, USA, (2009).

[13] Medha, V. W., Dr. Pradeep. M. P., and Hemant, K. A. Image Registration Techniques: An overview: International Journal of Signal Processing. Image Processing and Pattern Recognition; Vol. 2: No.3, September, (2009)

[14] Skykes, J. R., Brettle, D. S., Magee, D. R., and Thwites, D. I. (2009) Investigation of uncertainties in image registration of cone beam CT to CT on an image-guided radiotherapy system. Physics in medicine and biology. 54 (2009): 7263 – 7283.

[15] Wang, X. S., et al. A comparative study of three CT and MRI registration algorithms in nasopharyngeal carcinoma. Journal of Applied Clinical Medical Physics. 10 (2009), No. 2.

[16] Buhl, SK., Duun-Christensen, AK., Kristensen, BH., Behrens, CF. Clinical of evaluation of 3D/3D MRI-CBCT automatching on brain tumors for online patient setup verification – A step towards MRI – based treatment planning. Acta Oncologica. 49 (2010): 1085–1091.

[17] Fox, T., Huntzinger, C., Hohnstone, P., Ogunleye, T., and Elder, E. Performance evaluation of an automated image registration algorithm using an integrated kilovoltage imaging and guidance system. Journal of Applied Clinical Medical Physics. 7, No. 1 (2006): 97 – 104.

[18] Ryan, D., et al. Prostate positioning errors associated with two automatic registration based image guidance strategies. Journal of Applied Clinical Medical Physics. 10, No. 4 (2009): 165 – 176.

[19] IAEA. Commissioning and Quality Assurance of Computerized Planning Systems for Radiation Treatment of Cancer: TRS No. 430. Vienna, Austria. (2004)

[20] Hou, J., Guerrero, M., Chen, C., and Warren D.D. Deformable planning CT to cone-beam CT image registration in head-and-neck cancer. Medical Physics. 38 (2011): 2088 – 2094.

Vitae

Name	Miss Sumana Somboon
Date of Birth	August 12, 1985
Place of Birth	Bangkok, Thailand
Institution Attended	Faculty of Science, Prince of Songkla University, Bachelor of Science (Physics), 2007
Present Address	Study in Program of Master of Science in Medical Imaging, Department of Radiology, Faculty of Medicine, Chulalongkorn University.